

Challenges in crater chronology on Mars as Reflected in Jezero crater

Lior Rubanenko^{1,2}, Tyler M. Powell², Jean-Pierre Williams², Ingrid Daubar³,
Kenneth S. Edgett⁴, and David A. Paige²

¹Stanford University, Stanford, CA

²University of California, Los Angeles, CA

³Brown University, Providence, RI

⁴Malin Space Science Systems, Inc., San Diego, CA

Abstract

The age of a planetary surface may be inferred from the size frequency distribution of impact craters covering it. On Mars, the accuracy of this *crater chronology* technique may be compromised by past or present aeolian, fluvial and pluvial erosion and sedimentation. Here, we review how these processes influence the crater age of the surface, employing as a case study the floor of Jezero Crater, the landing site of the Mars 2020 Perseverance rover mission. We count craters and derive the retention ages of three prominent geologic units on the floor of Jezero, discussing some of the challenges faced during crater counting analysis. Our estimate for the retention age of the dark-toned floor unit is slightly younger compared to previous studies, and is sensitive to statistical outliers. These factors should be taken into account when calibrating the crater age of the surface of the unit with its measured radiometric age.

1 Introduction

All solid planetary bodies in the solar system are scarred by craters of meteoritic origin, relics of the disc of debris that orbited the primordial Sun (Spencer, 1937). Cratered terrains record impacts integrated throughout their geologic lifetime. As a result, the size distribution of craters imprinted on a planetary surface may be used to constrain its age, assuming the impact rate over time is known (Baldwin, 1949; Kreiter, 1960). This method, termed crater chronology, is rooted in the assumption that the size frequency distribution of craters on an initially smooth airless planetary surface closely follows the distribution of the impactors that formed them. However, many geologic processes impair our ability to perform crater chronology by affecting both production of new craters and removal of preexisting craters (Melosh, 1989; Neukum et al., 2001).

On the airless Moon, impacts are the main processes that affect craters erosion and morphology through impact gardening by meteorites and overprinting by larger craters and ejected materials. In the past, volcanism also contributed to removing craters from the surface, mainly through burial. On Mars, the observed crater size distribution is also influenced by the planet's atmosphere. This includes not only atmospheric breakup and

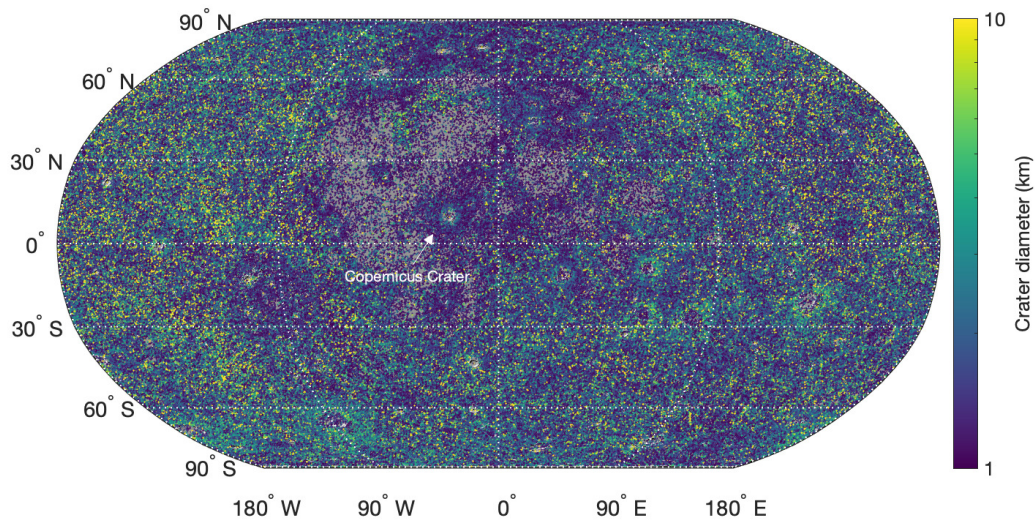


Figure 1: Impact craters > 1 km on the Moon, color-coded by diameter on a logarithmic scale and stretched for emphasis (Robbins, 2019). Typically, the areal density of lunar craters varies as a function of the age of the surface. Locally, secondary craters may increase the number of craters on the surface, affecting its model derived age (McEwen et al., 2005). For example, the dense population of secondary craters (secondaries; craters formed by fragments of the target material ejected by the primary impactor) around Copernicus Crater (10° N, -20° E) makes the surrounding surface appear significantly older than other parts of the lunar Maria despite its younger age (Robbins, 2019). The range of crater diameter (stretched here for emphasis) demonstrates the typical crater size varies quite significantly for different regions, where craters in the younger maria region tend to be slightly smaller (more purple) than craters in the highlands (more yellow).

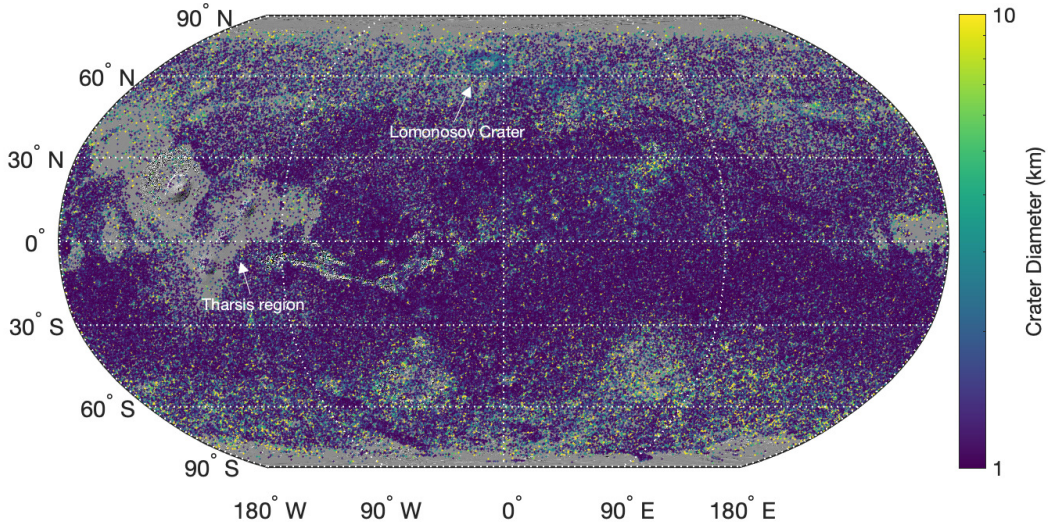


Figure 2: Impact craters > 1 km on Mars, color-coded by diameter on a logarithmic scale and stretched for emphasis (Robbins and Hynek, 2012a). Compared to the airless and mostly geologically inactive Moon (Figure 1), Mars shows evidence of volcanic (*e.g.* around Tharsis region) and atmospheric processes (*e.g.* ice near the poles) that change the crater areal density and size distribution both locally (such as around Lomonosov Crater) and on larger scales.

37 aeolian processes that can affect crater morphology over time (Ivanov et al., 1997; Popova
 38 et al., 2003), but also pluvial, fluvial and sedimentary processes such as erosion by rivers,
 39 lacustrine sedimentation or glacial activity that are only enabled by Mars' atmosphere [cite
 40 from the book: Viola+ 2020, Soare+ 2020, Gallagher+ 2020, Parker, 2020], and may bury
 41 or exhume impact craters (Milton, 1973; Lorenz and Lunine, 1996; Irwin III and Zimbelman,
 42 2012; Robbins and Hynek, 2012b). Consequently, while the size frequency distribution of
 43 craters on the Moon typically varies as a function of the age of the surface (Figure 1), on
 44 Mars, atmosphere-related processes may complicate this relationship. For example, note
 45 the latitudinal trend in both density and size distribution shown in Figure 2 which may
 46 be caused by infill of small craters (Dobrea et al., 2020). These add to local variations in
 47 crater density due to the presence of secondaries visible, *e.g.*, near younger large craters
 48 such as Lomonosov Crater (65° N, -10° E) or resurfacing by volcanism around Tharsis
 49 and Olympus Mons (eastwards of longitude 90° E, also see Figure 3). The influence of
 50 secondaries on the primaries distribution may increase in environments where ground ice
 51 promotes relaxation and decreases primary crater retention.

52 The various processes that affect the observed crater size distribution on Mars gave birth

53 to the concept of crater retention age (Hartmann, 1966, 2005) which represents the time
54 during which craters of some diameter have accumulated and retained. This includes, in
55 some cases, episodes of crater burial and exhumation (Malin et al., 2010).

56 In this manuscript, we review how the Martian environment affects the retention age of
57 geologic units on Mars, focusing on Jezero Crater, a ~ 40 km impact crater located in the
58 Nili Fossae region of Mars, the landing site of the Mars 2020 Perseverance rover mission.
59 Even before earning its name, Jezero Crater was frequently cited as a textbook example for
60 a developed martian lacustrine system (e.g Fassett and Head III, 2005; Ehlmann et al., 2008;
61 Schon et al., 2012; Goudge et al., 2012). The network of channels and valleys stretching
62 hundreds of kilometers into the crater remain convincing evidence for extended periods of
63 overland flow on Mars (Lapôtre and Ielpi, 2020). These rivers carried phyllosilicate clays,
64 which are known to preserve organic matter, from the environment outside Jezero into a
65 delta fan located near its north-western rim. This makes Jezero a promising candidate to
66 test the question of the past or present habitability of Mars. In addition, the rover is planned
67 to collect core samples from the floor of the crater that will be retrieved and shipped to
68 Earth by a future mission (Williford et al., 2018). Relating the absolute radiometric ages
69 of different geologic units within Jezero to their crater-derived retention ages will serve to
70 "calibrate" the planet's impact crater chronology. Consequently, constraining the crater-
71 age of the landing site and the surrounding region has implications for crater chronology
72 determinations throughout the planet.

73 This chapter is intended to be accessible to readers inexperienced in crater chronology.
74 We first review some basic concepts in crater chronology that will be employed throughout
75 the text. Then, we present the geologic setting of Jezero Crater and perform crater statistics
76 on three prominent geologic units found within in. Finally, we discuss how the surface
77 conditions on Mars may have affected the crater-derived age of these units.

78 2 Basic Concepts in Crater Chronology

79 2.1 Theory

80 Nearly a century ago, astronomers proposed that the origin of craters on the lunar surface
81 is meteoritic and not volcanic (Spencer, 1937). The formation process of craters from im-
82 pactors may be broadly divided into three stages (Melosh, 1989). In the first *contact and*
83 *compression* stage, the projectile transfers its kinetic energy to the target material, pushes
84 and compresses it. In the second *excavation* stage, material is expelled from the point of
85 impact by the nearly hemispherical shock wave. At the end of the excavation stage, a tran-
86 sient bowl shaped cavity forms that is much larger than the impactor itself. This cavity is
87 almost immediately altered by gravity in the last *modification* stage, and the crater obtains
88 a final, shallower shape.

89 The comprehensive statistical analyses of cratered surfaces on the Moon compiled by
90 Young (1940) and later by Kreiter (1960) and Hartmann (1964) provided the first quantita-
91 tive evidence for the meteoritic origin hypothesis. These studies found the size distribution
92 of craters $\sim 10 - 100$ km may be well-described by a power law, similar to the size distribu-
93 tion of asteroids and terrestrial meteorites (Brown, 1960). Around the same time, Hawkins
94 (1960), Anders (1965), Hartmann and Hartmann (1968) and others theorized collisional
95 cascades between asteroids form power-law distributed impactor sizes, leading to power-law
96 distributed impact crater sizes.

97 Adopting these ideas, we may mathematically describe the number of craters per unit
 98 area N with diameters $\geq D$ using a simple power law (Crater Analysis Techniques Working
 99 Group, 1979),

$$N(\geq D) = cD^{-b}. \quad (1)$$

100 where b is the slope of the production function in log-log scale and c is a coefficient that
 101 translates the distribution vertically, along the y-axis.

102 These basic concepts are demonstrated in Figure 3, where we show a cratered surface
 103 near Olympus Mons in panel (a) and the corresponding crater cumulative size distribution
 104 in panel (b). The crater size distribution of the surface in panel (a) is well represented by
 105 a power law size distribution. As expected, the normalized cumulative count values of the
 106 more heavily cratered region are higher than those of the less heavily cratered region.

107 Another way to represent the number of craters on the surface is by using a differential
 108 distribution; the number of craters in some diameter bin whose width is dD , divided by the
 109 bin size,

$$\frac{dN}{dD} = bcD^{-(b+1)} = \tilde{c}D^{-(b+1)}. \quad (2)$$

110 Yet another representation of cratered surfaces is called the incremental distribution, the
 111 absolute number of craters in a bin dD . The advantage of the incremental representation is
 112 that its slope, when using log-spaced diameter bins, is the same as that of the cumulative
 113 distribution. In panels (c) and (d) of Figure 3 we show examples of a differential and an
 114 incremental distribution.

115 For a non-zero flux of impactors, the number of craters on an initially crater-free surface
 116 will increase with time. As a result, measuring the coefficient c of a crater power-law size
 117 distribution is - at least conceptually - similar to measuring the relative age of the surface.
 118 In order to obtain the absolute age, c must first be calibrated for surfaces whose age was
 119 derived employing methods such as radiometric or cosmic ray exposure age dating of samples
 120 collected on the Moon. By using models that describe the impactor size distribution across
 121 the solar system and their respective impact probabilities for each planet, these absolute
 122 measurements can be extended from the surface of the Moon to the surface of other planets
 123 (e.g Ivanov, 2001; Stöffler and Ryder, 2001; Marchi et al., 2009; Le Feuvre and Wicczorek,
 124 2011).

125 Initially, The production rate of craters will closely follow the impact rate. As time
 126 passes, newly formed craters will superimpose existing craters. At some point in time, the
 127 crater population will become so dense that *any* new crater formed on the surface will
 128 replace craters that occupy an area equal to the area affected by the new crater. This stage
 129 is termed crater saturation (sometimes termed equilibrium); even though new craters form
 130 on the surface, the observed crater density does not increase (Baldwin, 1981; Melosh, 1989;
 131 Neukum et al., 2001). We note that in many studies the term *crater equilibrium* describes a
 132 state in which craters are formed at the same rate they are destroyed by any surface process.
 133 To avoid confusion, we adopt the term saturation

134 In many cases, crater saturation is described as a fraction of the *geometric saturation*, the
 135 number of craters that can be placed on an area fitted rim-to-rim in hexagonal close packing
 136 (Gault et al., 1974; Melosh, 1989). This stage may also be represented by a differential
 137 power-law coefficient ≈ 0.22 .

138 With that concept in mind, it is useful to consider an additional mathematical depiction
 139 of cratered surfaces that would help identify saturation: the R-plot (relative plot). To obtain
 140 the R-plot of a crater population, we divide the incremental distribution by a power law with

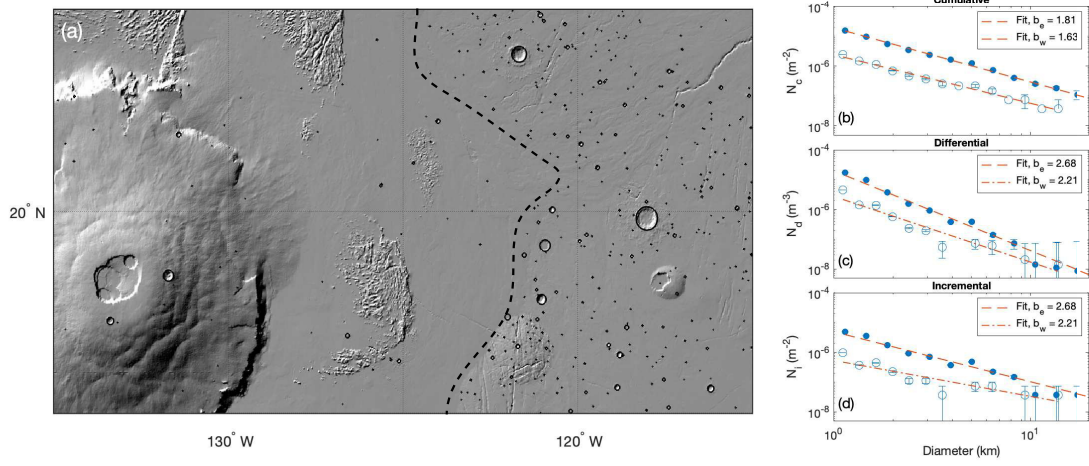


Figure 3: Shaded relief map (Smith et al., 2001) of cratered terrain that was recently resurfaced by volcanism, near Olympus Mons. (a) The lower crater density in the region closer to mount Olympus (west of $\sim 122^\circ$ W, also emphasized by the dashed line) indicates a more recent or extensive resurfacing relative to the region further away from the mount. (b) Cumulative (c) differential and (d) incremental size distributions with $\sqrt{2}$ logarithmic bin increments. Filled and empty circles show the distributions in the more heavily cratered region (east of the dashed line) and recently resurfaced region (west of the dashed line). b_e and b_w in the panels legends is the slope of the power law in log-log scale of the eastern and western crater distribution, respectively. Error bars are Poisson.

141 $b = 2$ (or the differential distribution by a power law with $b = 3$). In an R-plot, horizontal
142 lines represent size distributions in which craters in every bin occupy the same fraction of the
143 total area. As a result, the R-plot of surfaces in saturation will both be horizontal and have
144 R values of 0.22. Increasing/decreasing R lines represent crater cumulative distributions
145 whose incremental distribution exponent is $b < 2$ or $b > 2$, respectively. In panels (a-d) of
146 Figure 4 we show four example regions on Mars and the Moon. In panel (e) we show R-plots
147 for these regions, which demonstrates their age difference and proximity to saturation.

148 2.2 Practice

149 The guiding principle of crater chronology is relatively straightforward; with time, older
150 surfaces will experience more impacts and, as a result, will be more heavily cratered. This
151 concept is well demonstrated in Figure 3, which shows how the recently resurfaced region
152 surrounding Olympus Mons is nearly devoid of craters > 1 km compared to areas farther
153 away from it, and in Figure 4, which compares cratered surfaces of different ages.

154 In order to determine the age of a surface, it is necessary to find the size distribution of
155 the craters covering it. Traditionally, this *crater counting* technique is performed manually
156 by first dividing the surface into homogeneous geologic units and recording the diameters of
157 the visible craters within each unit (Greeley and Gault, 1970; Melosh, 1989; Neukum, 1984;
158 Michael and Neukum, 2010). In recent years, this process is gradually being replaced by
159 automatic detections that involve computer vision, machine and deep learning techniques
160 (e.g Barata et al., 2004; Stepinski et al., 2009; Silburt et al., 2019). It is, however, important
161 to note these algorithms often suffer from high false positive and false negative rate and
162 consequently treated with suspicion by experienced crater counters.

163 Detailed studies of cratered surfaces have found that the power-law assumption stated
164 above does not always accurately capture the shape of the crater size distribution over large
165 diameter ranges. This is in part due to the irregularities and the so-called "knees" in the
166 size distribution of the asteroidal bodies that form them (Fujiwara and Tsukamoto, 1980;
167 Rabinowitz, 1993; Stuart and Binzel, 2004). As a result, Neukum et al. (1975), Hartmann
168 (1981), Neukum et al. (2001), Hartmann and Daubar (2017) and others employed crater
169 counts to measure the size distribution of lunar craters and fit it with a piecewise power
170 law or a series of polynomials that more accurately describe its features. These elaborate
171 functions are termed *production functions*, and have since been updated using more recent
172 cratering data (Neukum and Ivanov, 1994; Hartmann, 1999; Marchi et al., 2009; Le Feuvre
173 and Wieczorek, 2011; Williams et al., 2014) and observations (Brown et al., 2002; Mainzer
174 et al., 2012). Over the years, these production functions have been adapted to date planetary
175 surfaces for which we have no radiometric ages such as Mars, Mercury and the moons of the
176 outer planets (e.g. Ivanov, 2001; Bierhaus et al., 2005; Marchi et al., 2009; Le Feuvre and
177 Wieczorek, 2011; Strom et al., 2011).

178 Graphically, production functions define lines termed isochrons, which represent the state
179 of a crater size distribution at some point in time. For example, in Figure 4 (e) we show how
180 isochrons derived from the Ivanov (2001) production function can aid in dating planetary
181 surfaces by matching them with a measured crater size distribution. Graphically, the size
182 distribution represented by the red dots better fits the contour defined by the 10^9 yr isochron,
183 while the size distribution represented by the blue dots better fits the contour defined by
184 the 3×10^9 yr.

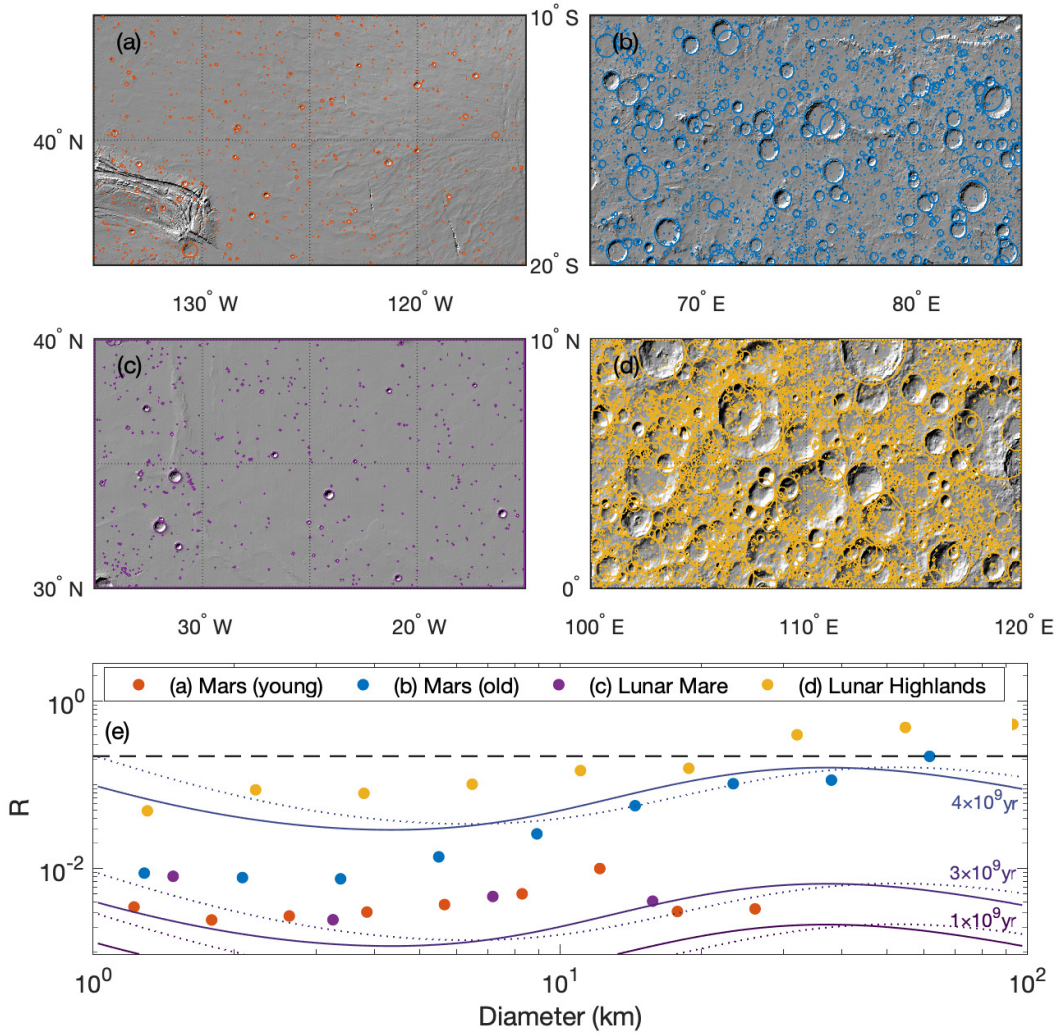


Figure 4: Four regions on the Moon and Mars showing different degradation states. (a) A region on Mars that was recently resurfaced showing lower crater density and smaller average crater diameter. (b) An older region on Mars shows the opposite. (c) A subset region of the lunar maria. (d) A subset region of the lunar highlands, which is an example for a surface close to crater saturation (indicated by the black dashed line). (e) R-plots for the different regions, with isochrons derived from the Ivanov (2001) model for Mars (solid lines) and Neukum et al. (2001) model for the Moon (dotted line).

185 3 Challenges in Crater Chronology in Jezero Crater

186 The methodology described above is idealized as it assumes only impacts can form and
187 erode craters. However, many surface processes can disguise themselves as impact craters;
188 it can be difficult to discern volcano pits, subsidence craters and lava vents from craters
189 formed by meteorites (Greeley and Gault, 1971; Blasius, 1976; Melosh, 1989). For example,
190 the cavities in the bottom left corner of Figure 3 (a) not marked by black circles are the
191 Olympus Mons summit calderae. At times, the geologic interpretation of what constitutes
192 an impact crater may significantly affect the crater retention age estimates (Robbins and
193 Hynek, 2012a). Additionally, spatial and temporal variations in bolide production or surface
194 properties can change the production function and affect the morphology of fresh craters,
195 and geologic and atmospheric processes may reduce the number of visible craters on various
196 scales by burial, exhumation, infill or erosion. Finally, on scales < 100 m, fluctuations in
197 atmospheric thickness may also affect the crater size distribution (Chappelow and Sharpton,
198 2006).

199 In the following section we discuss how these complications are expressed in Jezero crater,
200 the landing site of the Mars 2020 Perseverance rover mission.

201 3.1 The Geology of Jezero Crater

202 Nearly two decades ago, instruments on board several Martian orbiters recorded a widespread
203 network of valleys in the Nili Fossae region, leading into two deltaic deposits located near
204 the northwestern wall of a ~ 40 km impact crater (18.4° N, 77.55° E) (Fassett and Head III,
205 2005). Further morphological analysis suggested the rivers that formed these valleys poten-
206 tially filled the impact crater until its eastern rim was overtopped and breached, creating
207 an outlet valley. These observations, along with earlier studies (De Hon, 1992; Cabrol and
208 Grin, 1999), provided additional evidence for the existence of developed lacustrine systems
209 on early Mars, earning the crater the name Jezero ("lake" in many Slavic languages).

210 In 2018, it was announced Jezero was selected as the landing site for the Mars 2020 mis-
211 sion (Grant et al., 2018). Jezero was selected mainly due to its distinct delta fan deposits
212 that showed phyllosilicate mineral enrichment (Ehlmann et al., 2008; Goudge et al., 2017).
213 The drainage basins for the deltas, which extends well into the Nili Fossae grabens, poten-
214 tially funneled diverse minerals such as clays and organic materials into Jezero, making it
215 a promising candidate to address the question of the past or present habitability of Mars
216 (Goudge et al., 2015; Grant et al., 2018).

217 Detailed geomorphological analysis (Goudge et al., 2015) of Jezero and the drainage
218 basin surrounding it revealed layered geology characteristic of lacustrine systems (Figure
219 5). Within the crater, the oldest layer is the rim and wall material which is covered in most
220 places by dust. Small exposures reveal a distinct spectra indicative of Mg/Fe-smectite.
221 Stratigraphically above the Rim and Wall layer are the Mottled terrain unit and the light-
222 toned floor (LTF) unit, which is covered in many areas by dunes. The dunes covering the
223 LTF unit present a strong spectral signature consistent with Olivine, while the unit itself
224 presents absorptions identified as hydrated carbonates, especially magnesite. Patches of the
225 mottled terrain unit are found both inside the crater and in the surrounding region, and is
226 stamped with circular features likely to be degraded impact craters.

227 Perhaps the two most intriguing geologic units in Jezero Crater are the north and west
228 delta deposits (Goudge et al., 2015). These units, whose sediment volume is estimated at
229 ~ 5 km³, were deposited in Jezero during the crater's stage as an extensive paleolake. The

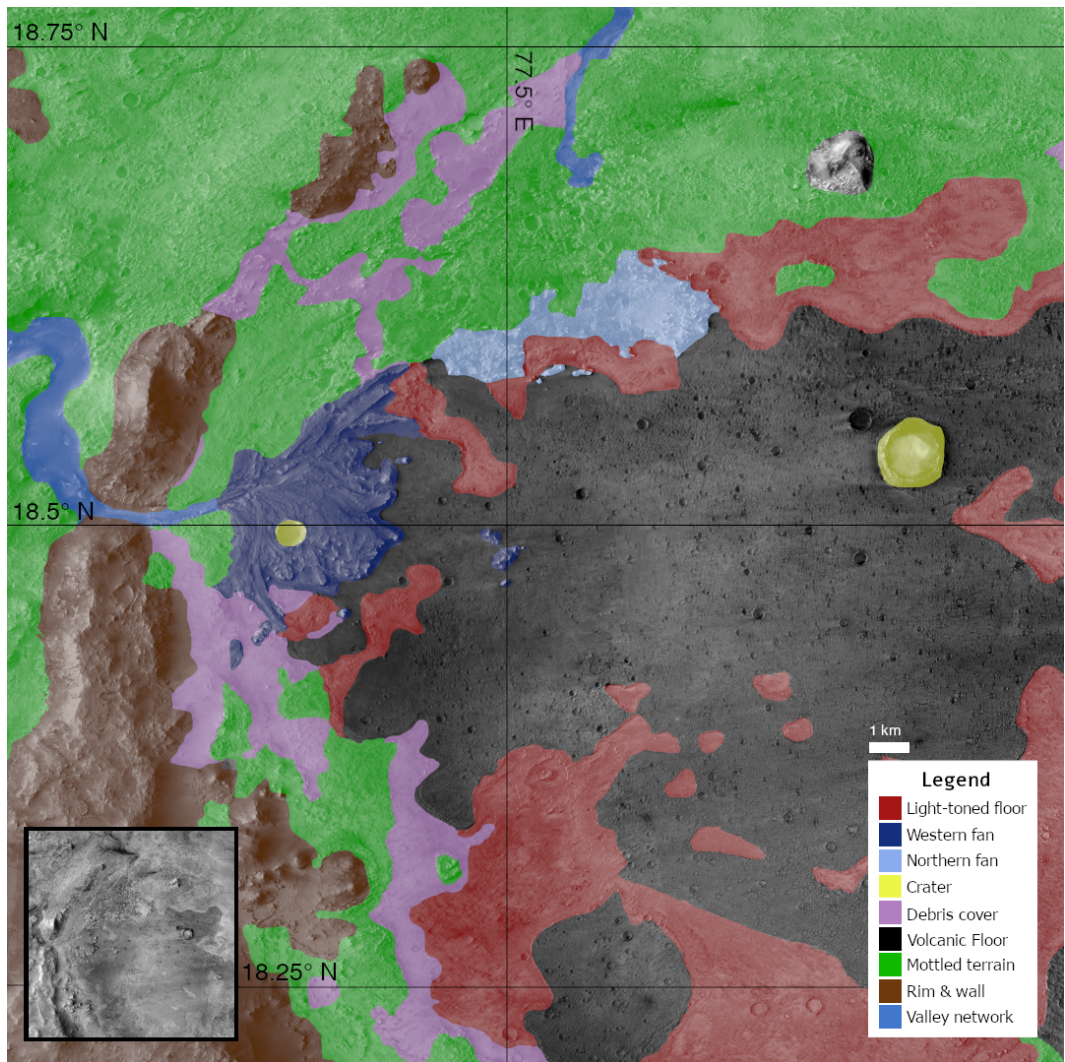


Figure 5: Jezero Crater geologic map overlaid on a basemap of the Jezero Crater mosaic captured by the Mars Reconnaissance Orbiter Context Camera (Malin et al., 2007). See section 3.1 for a description of each geologic unit. Bottom left: grayscale minimap of Jezero crater. Map was modified and enhanced from the original compiled by Goudge et al. (2015).

230 amount of material emplaced in the deltas implies the duration of inflow into Jezero lake
231 was probably substantial (Fassett and Head III, 2005; Lapôtre and Ielpi, 2020), testament
232 of the climatic conditions in the Nili Fossae valley during the Noachian Period (Fassett and
233 Head III, 2005). Of the two deltas, the northern fan is more eroded than the western fan
234 which still preserves the inlet channel that once formed it.

235 The most pervasive unit on the crater floor is termed the volcanic floor unit (Goudge
236 et al., 2015). This dark-toned, smooth layer was emplaced directly upon the light-toned
237 floor unit and was interpreted to embay the two delta fan deposits (Goudge et al., 2012).
238 Spectroscopic analysis shows absorption near $1\ \mu\text{m}$ and $2\ \mu\text{m}$, which may hint at the presence
239 of olivine and pyroxene (Goudge et al., 2015). More recent studies have indicated the
240 formation of the volcanic floor unit and its depositional history may be more confounding
241 than previously thought (Golder et al., 2020; Kah et al., 2020; Baum and Wordsworth,
242 2020; Schuyler et al., 2020). To avoid the interpretive nomenclature, we call it hereafter
243 the “dark-toned floor unit”, taking into account these types of rock units can potentially be
244 found to be sedimentary (Edgett and Malin, 2014).

245 Due to Jezero’s stratigraphy, constraining the age of the dark-toned floor unit using
246 crater statistics may help constrain the time in which its lake disappeared (Shahrzad et al.,
247 2019). Somewhat fortunately, the unit appears to preserve continuous crater production,
248 which may indicate its crater retention age will better correspond to its true (radioemetric)
249 age compared to typical martian terrains.

250 3.2 Small Crater Statistics Within Jezero Crater

251 To perform our analysis we compiled a catalog of craters within Jezero, nearly complete down
252 to $\sim 50\ \text{m} - 70\ \text{m}$ diameter, as measured by the deviation from power law. The purpose of
253 this catalog is not only to provide information towards the future Mars 2020 mission, but
254 also to demonstrate how various surface processes on Mars affect the age determined by
255 crater chronology.

256 We first review four cratered geologic units within Jezero Crater: the dark-toned floor
257 unit, the western and northern delta units and the light-toned unit. For each unit, we fit an
258 age employing a crater chronology model appropriate for our diameter range. In the section
259 following we discuss the various geologic processes that may affect the age determined by
260 the model, and how those may be addressed.

261 For consistency, we have elected to retain the names of the geologic units as they appear
262 in previous works (Schon et al., 2012; Goudge et al., 2015, 2017), noting in some cases they
263 may not reflect the true nature of the unit that are yet to be revealed by the Mars 2020
264 mission.

265 3.2.1 The Dark-Toned (Volcanic) Floor Unit

266 Over the last decade there has been some discussion over the age of the dark-toned floor unit
267 of Jezero crater. Early works derived ages that differ by a factor of 2, from 1.4 Ga (Schon
268 et al., 2012) to 3.45 Ga (Goudge et al., 2012). It should be noted these studies were not
269 focused on Jezero but on martian lacustrine systems in general, and employed low resolution
270 imagery data which limited the size of counted craters. More recently, Shahrzad et al. (2019)
271 were able to better constrain the crater-age of the dark-toned deposit to $\sim 2.6\ \text{Ga}$ using 187
272 craters with diameters $> 177\ \text{m}$.

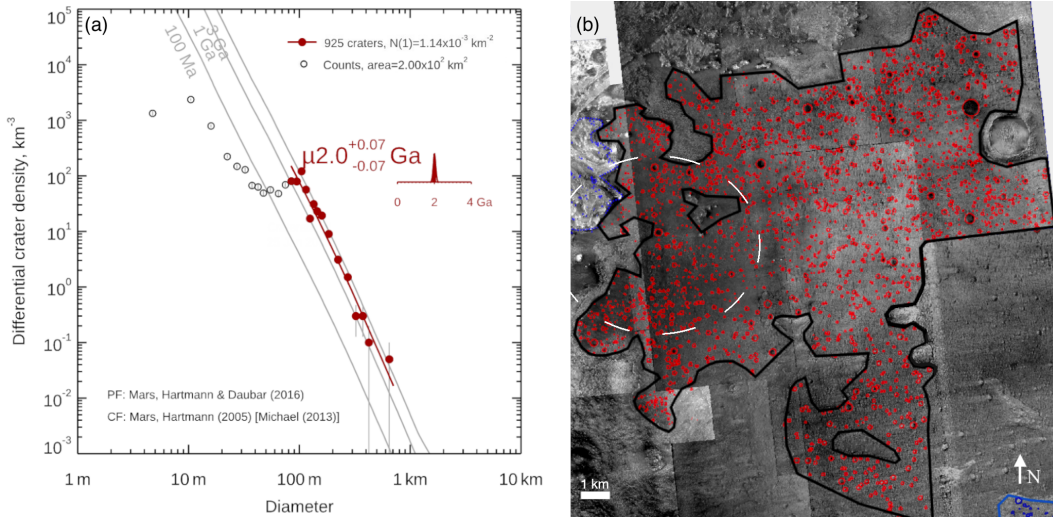


Figure 6: (a) Crater statistics on a subset region of the dark-toned (volcanic) floor unit of Jezero Crater, close to the landing site ellipse near the western delta. By fitting a model age appropriate to our diameter range and Poisson timing analysis probability density function (Michael et al., 2016; Hartmann and Daubar, 2017), we derive an age estimate of $\sim 2.0 \pm 0.07$ Ga. We only fit a model age to diameters greater than the rollover point (filled circles). (b) The spatial distribution of the craters on the dark-toned floor unit. The black line shows the edge of the subset region considered to make the differential plot in (a) and the white ellipse shows the approximate Mars 2020 landing site ellipse.

273 Power law statistics are sensitive to outliers. As a result, Shahrzad et al. (2019)’s age
 274 determination may be influenced by the small range of diameters they considered, that
 275 spans less than an order of magnitude. Additionally, given the thickness estimates of the
 276 dark-toned floor unit (10 – 30 m, Schon et al. (2012); Shahrzad et al. (2019)), it is possible
 277 that some of the larger craters in their sample predate the emplacement of the dark-toned
 278 floor.

279 In order to reproduce the results of Shahrzad et al. (2019), we expand the analyzed
 280 diameter range by comparing image sets with different image saturation and illumination
 281 conditions obtained by the High Resolution Imaging Science Experiment (HiRISE, McEwen
 282 et al. (2007)). In total, we surveyed 2859 craters formed on the dark-toned unit, whose
 283 diameters span two orders of magnitude: 5 – 670 m.

284 To perform our age analysis we chose a contiguous area ~ 200 km², excluding ”islands”
 285 belonging to other geologic units (see Figure 5 for reference). We derive differential crater
 286 size distributions and fit them with a model (Hartmann and Daubar, 2017) employing Pois-
 287 son timing analysis (Michael et al., 2016) using the *Craterstats* software package (Michael
 288 and Neukum, 2010). In Figure 6 we show our crater map and derived differential crater size
 289 distribution, which is composed of two branches that follow different isochrons - possibly
 290 indicating recent resurfacing (see section 3.3.1 for discussion).

291 In order to calculate the retention age of the dark-toned floor unit, we fit 925 craters
 292 85 m – 670 m with a chronology model appropriate for decameter sized craters (Hartmann
 293 and Daubar, 2017). The range of crater diameters in our sample was chosen to include

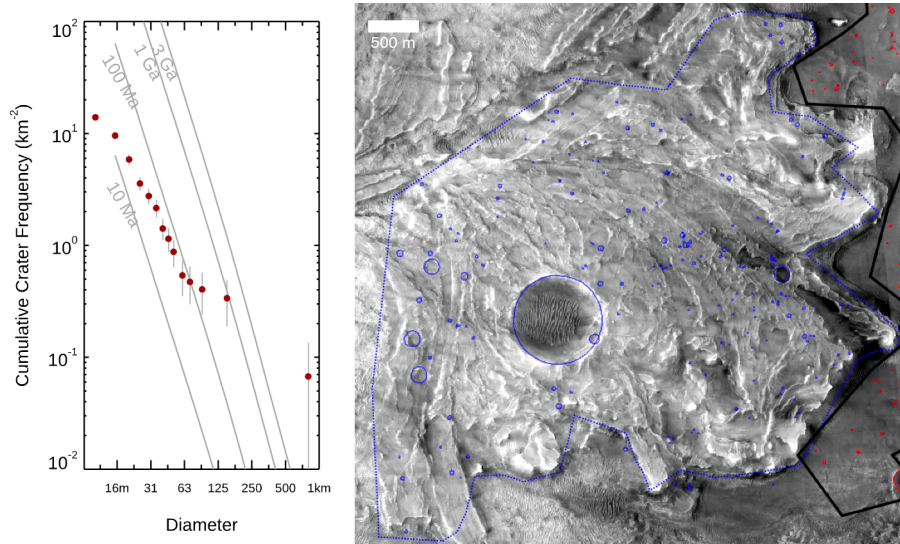


Figure 7: Crater statistics on the western delta fan unit, which does not preserve craters as well as the dark-toned (volcanic) floor unit.

294 craters that would likely postdate the formation of the dark-toned floor unit based on its
 295 estimated thickness (10 – 30 m, Schon et al. (2012); Shahrzad et al. (2019)), and the rollover
 296 diameter of the population. Assuming an initial depth/diameter ratio of 0.2, it is relatively
 297 safe to assume craters whose diameters < 200 – 300 m do not predate the dark-toned unit.

298 To estimate the rollover diameter on the dark-toned unit, we employ bootstrapping as
 299 explained in section 3.3.1. The age we determine for the dark-toned floor unit is 2.0 ± 0.07 Ga,
 300 slightly younger than the age obtained by Shahrzad et al. (2019) using the same model but
 301 a more restricted diameter range, 2.6 ± 0.2 Ga. It is important to note these ages most likely
 302 represent the crater retention age rather than the age of the unit (Hartmann, 1966). This
 303 is further discussed in section 3.3.1.

304 3.2.2 The Northern and Western Delta fan Units

305 Some of the stratigraphic evidence suggests both delta fan units precede the dark-toned floor
 306 unit, which embays them in many locations (Goudge et al., 2015). Unlike the dark-toned
 307 surface, the delta fans do not efficiently retain small craters, potentially due to the target
 308 material’s higher susceptibility to erosion (Schuyler et al., 2020) or physical characteristics,
 309 which influence the crater dimensions during formation (see section 3.3.4).

310 The double-branched size distribution of craters on the western delta fan of Jezero (\sim
 311 17 km^2) is likely evidence for aeolian resurfacing, which is indicated by many eroded and
 312 shallow (buried) craters on the unit. Belva Crater, the largest crater on the delta unit,
 313 appears to postdate its formation, and most likely indicates the unit is a few Ga old, in
 314 agreement with the eroded state of craters on scales 100 – 200 m and models of channel
 315 infill and subsequent erosion (Goudge et al., 2018; Salese et al., 2020). The smaller craters
 316 on the western delta unit approximately follow the 100 Ma isochron (Figure 7) much like
 317 the craters on the dark-toned floor unit.

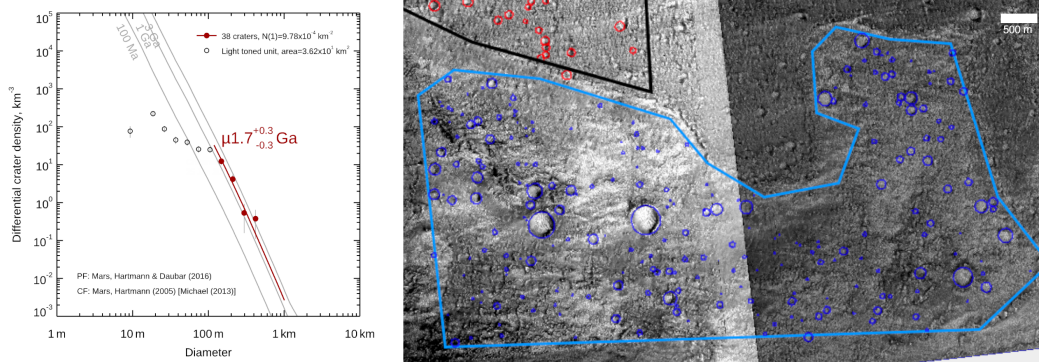


Figure 8: Crater statistics on the light-toned unit. Much like the delta fan units, the light-toned unit does not preserve craters well due to its extensive dune field.

318 The northern delta fan is significantly more eroded than the western delta fan (Goudge
 319 et al., 2015). This unit shows little evidence for impact cratering, where the largest crater-
 320 like depressions no larger than ~ 50 m. As a result, and while the geologic evidence suggests
 321 it is older than the dark-toned floor unit, the northern delta fan cannot be dated by using
 322 crater counting. For the same reason, the lower crater density on the northern delta does
 323 not necessarily imply it is younger than the western delta.

324 3.2.3 The Light Toned Floor

325 The extent of Jezero’s delta fan units indicates the crater’s lacustrine system has potentially
 326 been active for extended periods of time (Goudge et al., 2017). Consequently, it is not
 327 surprising that the spectroscopic analysis conducted by Goudge et al. (2015) and others
 328 found great diversity in the types of geologic units on the crater floor. Jezero’s light-toned
 329 floor is morphologically different than the dark-toned floor unit and is covered by several
 330 dune fields. To determine the retention age of this unit, it is necessary to find a subset region
 331 that contains craters that are large enough to survive erosion caused by the likely granular,
 332 dune-covered, target material and subsequent aeolian erosion and burial. In Figure 8 we
 333 derive the model age of the light-toned floor using 232 craters on our chosen subset region,
 334 whose area is 36.16 km^2 . Other parts of the light-toned unit either were not as contiguous or
 335 did not have enough craters to perform a statistically significant age estimate. We find that
 336 while the depositional age of the unit is greater than that of the dark-toned floor unit, its
 337 model age is slightly younger, 1.7 Ga. This demonstrates well the concept of retention age
 338 (Hartmann, 1966) where the crater-age of the surface is affected by processes that occurred
 339 (or are still occurring) after the surface had formed.

340 The differential crater size distribution on the light toned floor unit reveals again craters
 341 that follow two different isochrons. It is interesting to note that the younger branch of the
 342 distribution (at smaller diameters) follows a similar isochron to the one followed by the
 343 branches of the dark-toned floor unit and the delta floor unit. The potential implications
 344 of this observation will be discussed in the next section.

345 **3.3 Analysis: Challenges in Crater Chronology Within Jezero Crater**

346 **3.3.1 How do Conceptual Challenges in Crater Chronology Affect the Modeled** 347 **age?**

348 The age difference (approximately 0.5 Ga) between our analysis and the one performed
349 by Shahrzad et al. (2019) using the same chronology and production functions does not
350 necessarily suggest disagreement. Rather, it emphasizes a fundamental challenge in crater
351 chronology - that only rarely will two crater counting efforts return the exact same result.
352 This is especially true within more limited regions that are sensitive to erosion, such as
353 Jezero Crater.

354 The floor of Jezero crater is a textbook example for some of the challenges in crater
355 counting on Mars, where aeolian landforms often create closed shapes (in map view) that
356 imitate the circular shape of craters. In Figure 9 we annotate a few of these features,
357 which resemble impact craters in their general shape. Even though these features could be
358 identified as craters, careful examination shows their walls are a part of the elongated aeolian
359 features that cross the scene diagonally from top to bottom. This example emphasizes crater
360 counting is often prone to observation biases and personal experience (Greeley and Gault,
361 1970). As a result, it is important that a rigid set of criteria is defined during crater
362 chronology studies, which defines what feature to classify as impact craters. For example,
363 our criteria for classifying a depression as an impact crater is a closed shape (in map view),
364 circular (or nearly-circular) rims and a smooth floor. To further rule out false positives, we
365 compared several HiRISE images taken in different illumination conditions.

366 Different classification criteria may lead to different age determination, even when using
367 the same model. To demonstrate this, we fit craters in the diameter range considered
368 by Shahrzad et al. (2019) with the same chronology model as above, this time removing
369 seven craters that only loosely match our classification criteria. In Figure 10 we show these
370 craters along with the fitted cumulative plot model age, which shows removing them from
371 our sample decreases the modeled age by 200 Ma. When removing the same features from
372 our original fit that contains a greater number of small craters, the fitted age only changes
373 by $\sim 1\%$.

374 Having said that, and since this study focuses on challenges in crater chronology, it is
375 worthwhile to discuss how the Shahrzad et al. (2019) methodology differs from the one we
376 employed here. In their survey, Shahrzad et al. (2019) noted the lower limit for considering
377 craters useful for dating is not a factor of the image resolution (a few m/px) but of small scale
378 geological processes that accelerate crater erosion. Based on the rollover diameter of three
379 subregions of the dark-toned floor unit, they found the crater size distribution deviates from
380 the production function between 50 – 100 m and concluded that counts of craters < 100 m
381 are significantly affected by erosion or coverage. As a result, and due to additional spatial
382 non-uniformity more prevalent in smaller craters, they only counted craters > 177 m. This
383 limited diameter range could affect the derived crater age of the dark-toned floor unit not
384 only by increasing the variance associated with a smaller sample size; some of the counted
385 craters whose depth is equivalent to the estimated thickness of the unit (10 – 30 m, Schon
386 et al. (2012); Shahrzad et al. (2019)) could have, in theory, preceded its emplacement.

387 In an attempt to increase the survey diameter range and achieve more statistically ro-
388 bust results, we constrain the rollover diameter of craters using bootstrapping (Efron and
389 Tibshirani (1985), see also Figure 11). Bootstrapping is a well-known statistical method
390 for measuring the properties of estimators of a dataset by randomly sampling it with re-
391 placement. Instead of describing the data using a single value, bootstrapping could add

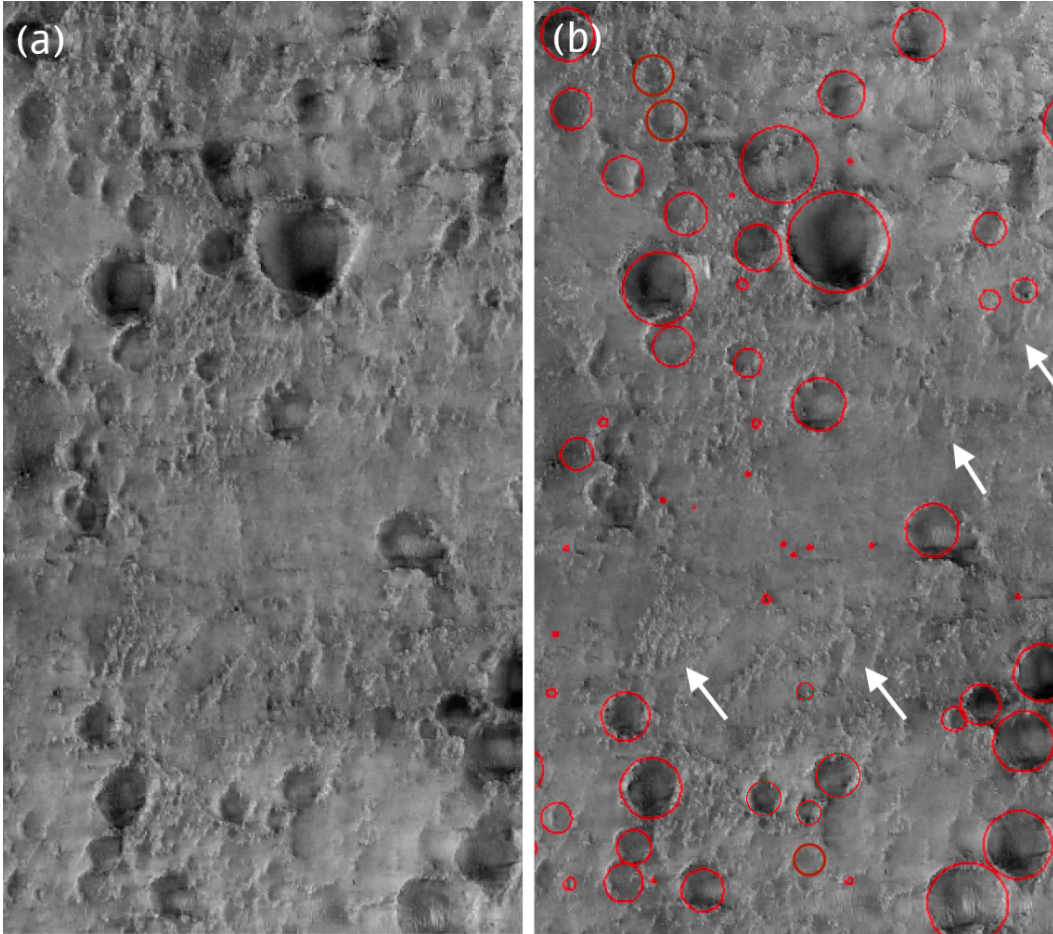


Figure 9: Distinguishing between impact craters and other depressions with a closed shape in map view is often difficult, and may pose a serious challenge in the data collection (crater counting) stage. Red circles show features identified as impact crater by comparing several HiRISE images. White arrows show a few examples for features that may resemble craters, but were not counted in our survey. Our criteria for identifying depressions as impact craters are a closed, circular shape in map view and smooth floor. For example, the flat depression at the center left border of the image may be a heavily eroded, infilled crater - but was not counted as one.

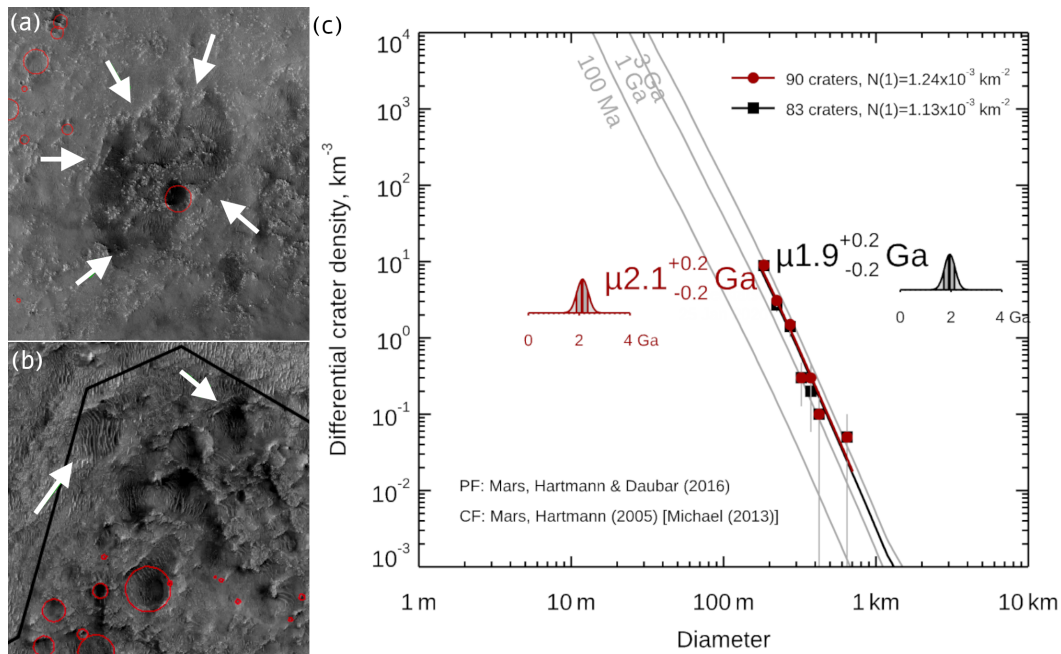


Figure 10: Including small craters in age determination can help resolve classification ambiguities that affect the model age. (a, b) Depressions ruled out as craters (white arrows) in this study, but counted as craters in previous studies (Shahrzad et al., 2019). (c) Here we show that if the sample only includes craters > 177 m (as in Shahrzad et al. (2019), however counted over a smaller region), removing seven ambiguous depressions (panels a, b) that may be classified as craters change the model age (red vs. black lines) by $\sim 10\%$. If the same seven large craters are removed from the fit in Figure 6 that contained an order of magnitude more craters the modeled age does not change.

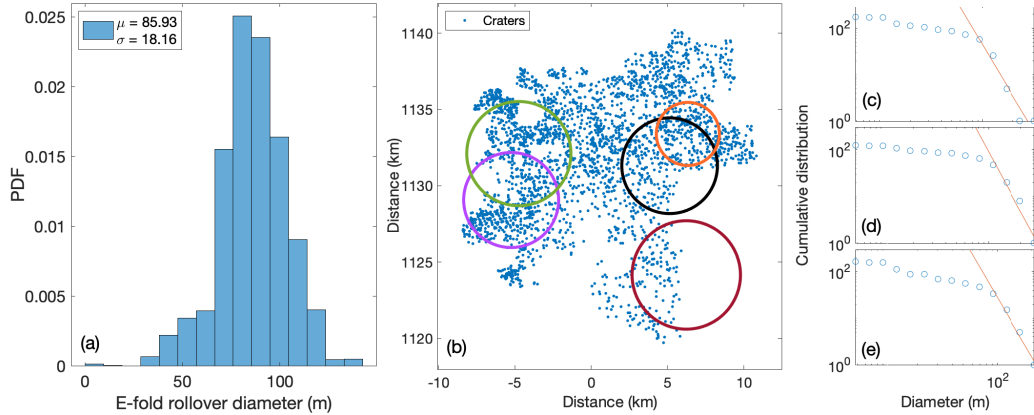


Figure 11: We constrain the rollover diameter of the crater size distribution using bootstrap analysis to be $\sim 85 \pm 18$ m. (a) The distribution of the rollover diameters over 5000 iterations, each containing at least 50 craters. Values in legend indicate the mean and standard deviation of the bootstrap distribution. (b) The spatial distribution of craters within Jezero’s dark-toned (volcanic) floor unit. Circles show a few example iterations of our bootstrap model used to cookie-cut craters and make the distribution in panel (a). (c-e) The power law size distribution for several example iterations. We first fit a power law to the right-hand branch of the size distribution, and calculate the difference between the fit and size distribution. The rollover diameter is estimated as the diameter in which this difference decreases e-fold.

392 information about the spatial variability of the sample bias or variance.

393 We create circular boolean masks with whose radii and position are drawn from a uniform
 394 distribution. We first choose the circle radius between 3 km and 5 km, and then randomize
 395 its position such that its entire area is contained within the floor unit. In each of the 5000
 396 bootstrapping iterations, we calculate the rollover diameter defined as the e-fold difference
 397 between the power-law part of the size distribution and the part deviating from that power
 398 law. We discard bins with < 50 craters. In Figure 11 we show the mean rollover diameter
 399 based on our analysis is $\sim 85 \pm 18$ m, and consequently choose to use craters whose diameter
 400 > 85 m. Our method could be utilized as a robust estimate of the rollover crater diameter
 401 in other cases.

402 3.3.2 Is the Dark-Toned (Volcanic) Floor Unit Contaminated by Secondary 403 Craters?

404 The areal density of craters on the dark-toned floor unit varies quite significantly, with what
 405 appears to be a decreasing east-west density gradient (Figure 12 (a)). The higher crater
 406 density in the northeastern part of the dark-toned floor was also noted by Shahrzad et al.
 407 (2019), who suggested a few possible causes, among which is contamination by secondary
 408 craters.

409 The question of whether contamination by secondary craters can potentially affect the
 410 surface age derived from crater chronology is an actively researched topic in planetary sci-
 411 ences. Observations conducted by Shoemaker (1965) on Mare Cognitum on the Moon have

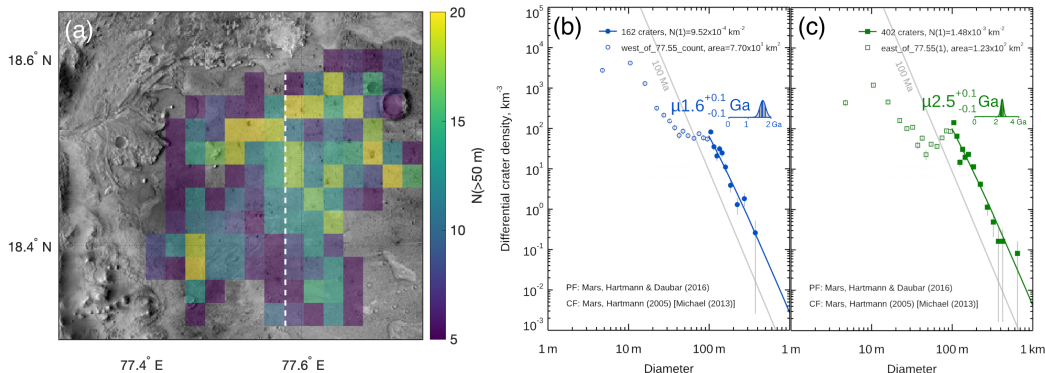


Figure 12: Variations in crater size distribution across the dark-toned (volcanic) floor unit. (a) The density of impact craters > 50 m on the mafic floor unit is higher in the north-eastern part of the basin divided into equal area bins $\sim 1 \times 1$ km. (b,c) Differential distribution of craters in the western side (b) and the eastern side (c) of the dark-toned floor unit, also emphasized by the white dashed line. The eastern and western crater size distributions are different both in the absolute crater density, but also in the average crater diameter, which is nearly double in the eastern side. Using the Kolmogorov-Smirnov test we reject the null hypothesis that the craters from both sides of Jezero originate in the same distribution ($p < 0.01$).

412 revealed a production function whose slope exponent for craters < 1 km is significantly
 413 steeper than the average slope in the lunar mare previously estimated by Hartmann (1964)
 414 and others for craters > 1 km. Later studies (Wilhelms, 1976; Schultz and Singer, 1980)
 415 further explored the spatial characteristics of secondary craters clusters and found a signifi-
 416 cantly steeper slope of ~ 4 and a shallower, more elliptical morphology due to the typically
 417 more oblique impact angle and generally lower impact velocity. Due to the steeper slope of
 418 the secondary size distribution compared to the primary size distribution, it was speculated
 419 that secondary craters could be significantly more numerous at smaller sizes than primary
 420 craters and affect the modeled age (Shoemaker, 1965; Soderblom et al., 1974).

421 During the past two decades, studies have suggested some km sized craters on Mars such
 422 as Zunil Crater (~ 10 km) may produce up to tens of millions of secondaries that extend
 423 hundreds of crater radii away from the primary impact (McEwen et al., 2005; Preblich
 424 et al., 2007). While this somewhat alarming result seems to imply secondaries may have
 425 a large cumulative effect on the average crater size distribution, more recent analyses have
 426 concluded that the majority of secondary craters on the Moon and Mars form close to the
 427 primary crater or along rays (Quantin et al., 2016; Williams et al., 2018; Bierhaus et al.,
 428 2018). However, the contribution of distant secondaries to the crater production function is
 429 still unclear. This topic is reviewed in depth in (cite Powell et. al chapter from the book).

430 We verify the observation that craters on the eastern side of the dark-toned floor are
 431 denser than craters in the western part using a Kolmogorov-Smirnov (K-S) one-tailed test
 432 (Massey, 1951), and reject the null hypothesis that craters in two sides of the floor unit
 433 come from the same distribution ($p < 0.01$, also compare lines in panels (b,c) of Figure 12).

434 It appears both visually and statistically that the crater density is higher in the eastern
 435 part of the dark-toned floor unit, but the reason behind this higher density is puzzling and

436 poorly understood.

437 The craters in the northeastern part of the dark-toned floor unit do not resemble a field of
438 secondary craters, with no immediately identifiable clusters or crater chains. Additionally,
439 craters in that area do not appear to be more elliptical or shallower compared to other parts
440 of the unit (see examples for distinctive secondaries fields in Robbins and Hynek (2011)) and
441 it does not appear that Jezero Crater is located near a large recent primary crater that may
442 have contaminated it with secondaries (Robbins and Hynek, 2014). However, contamination
443 by secondaries ejected from more distant basins cannot be completely ruled out.

444 Visually, the region with lower crater density in the western part of the dark-toned floor
445 unit resembles the eroded delta fragments in tone and smoothness more than it resembles
446 the dark-toned floor unit in the eastern, more heavily cratered side (Figure 13). This
447 leads us to speculate the reason for these patches of low crater density is that they were
448 exhumed from underneath the delta deposits which eroded and disappeared with time, or
449 that increased aeolian erosion on the western side of the crater removed material from the
450 delta fragments (blue islands near the center of Figure 5) onto the volcanic floor unit, burying
451 craters (Sweeney et al., 2018; Day and Dorn, 2019; Warner et al., 2020).

452 We finally note that in contrast to the visual geomorphological evidence, the crater size
453 distribution shown in Figure 6 may in fact support the hypothesis of contamination by
454 secondaries, due to the apparent excess of craters 100 – 300 m relative to craters > 300 m
455 that follow a younger isochron. It should be noted, however, that the limited number of
456 craters > 300 m reduces the statistical significance of this claim.

457 3.3.3 How do Aeolian Erosion and Infill Affect the Crater Size Distribution?

458 Many geologic processes may fade or erase craters: mechanical impact gardening (Gault
459 et al., 1974; Fassett and Thomson, 2014), seismically induced mass wasting (Richardson Jr
460 et al., 2005), exospheric ice (Deutsch et al., 2018; Rubanenko et al., 2019) or volcanic infill
461 (Hartmann, 1999; Edwards et al., 2014). On Mars, erosion is further accelerated by aeolian
462 processes fueled by Mars’ atmosphere (Neukum et al., 2001; Hartmann and Neukum, 2001;
463 Smith et al., 2008; Grotzinger and Milliken, 2012; Michael, 2013). In some cases, the crater
464 size distribution preserves erosion and resurfacing events that tend to have a greater effect
465 on the smaller, shallower depressions (as seen, for example, near Olympus Mons in Figure
466 3).

467 On a differential plot, the size distribution of an eroded or infilled population of craters
468 appears like a discontinuity whose branches follow different production function isochrons,
469 as fresh craters form where previous craters are lost (see, for example, Figures 6, 8 or 12,
470 and additional examples in Melosh (1989); Hartmann and Neukum (2001)). The model
471 age of the older branch may help constrain the age of the unit, while the model age of the
472 younger branch may help constrain the time at which the partial resurfacing event occurred
473 (Michael, 2013).

474 The effect of resurfacing on the crater age of a geologic unit may be seen by comparing the
475 crater size distributions analyzed above: even though the stratigraphic relations interpreted
476 by Goudge et al. (2015) would imply the delta unit precedes the dark-toned floor unit,
477 its eroded or infilled crater size distribution appears to represent a significantly younger
478 retention age. The same is true for the light-toned floor unit, in which aeolian features may
479 have affected the crater size distribution by removing or eroding craters. It is also interesting
480 to note the younger branch of all the surveyed units in Jezero Crater follows approximately
481 the same isochron, 10 – 100 Ma. This may imply a geologic process erased craters on scales

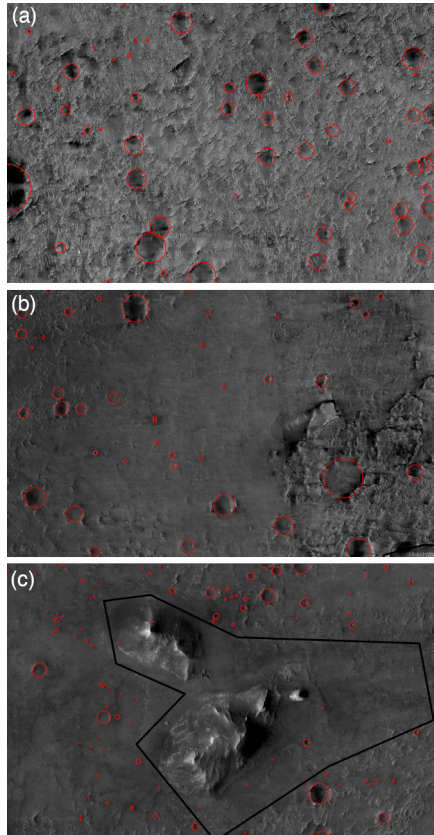


Figure 13: (a) A subset from the eastern side of the dark-toned (volcanic) floor unit. (b) A subset from the western side of the dark-toned floor unit. (c) An eroded delta deposit. Even though it was identified to be part of the dark-toned floor unit, panel (b) appears more muted, and visually resembles the delta deposit in panel (c) more than it resembles the dark-toned unit in (a). This may imply the area in the western part of the dark-toned floor unit was once covered by delta deposits similar to (c) that had nearly completely eroded with time.

482 < 100 m across all the geologic units of Jezero.

483 Some of the disagreement between this survey and previous surveys (Shahrzad et al.,
 484 2019; Schon et al., 2012; Goudge et al., 2012) may stem from the limited count area. Sur-
 485 veying limited count areas increases the statistical uncertainty in the derived model age
 486 due to the smaller sample size and the natural spatial variability that exists even within
 487 a single geologic unit (Pasckert et al., 2015; Williams et al., 2018). As resurfacing tends to
 488 affect smaller craters more than larger craters, its influence grows when the surveyed area
 489 is small (Warner et al., 2015). More recent probabilistic models (Palucis et al., 2020) have
 490 determined the highest uncertainty occurs for surfaces whose age is ~ 2 Ga, which is close to
 491 the crater age of the dark-toned floor unit. For landscapes that exhibit limited erosion, an
 492 accurate surface age may be predicted on the condition that the ratio of the square root of
 493 the tested area to the minimum crater diameter does not exceed ~ 200 (Palucis et al., 2020).
 494 This condition is met for our survey of the dark-toned floor unit but not for previous surveys
 495 (Shahrzad et al., 2019). However, when considering a moderate erosion rate of 25 nm y^{-1} ,
 496 a much greater minimum area of 10^4 km^2 is required. This should be considered if a sample
 497 obtained from the dark-toned floor unit will be used in the future to calibrate Mars’s crater
 498 chronology.

499 3.3.4 How do the Target Material Properties Affect Crater Chronology?

500 The previous sections have dealt with the evolution of cratered surfaces over time and the
 501 concept of crater retention age. In addition to these challenges, the geological diversity of
 502 Mars - a consequence of its prolonged history of surface water and active atmosphere - has
 503 led to significant differences in the target material properties of cratered terrains, thereby
 504 affecting their formation diameters and size distribution, and the derived retention ages.
 505 This is emphasized within fossilized lacustrine systems such as Jezero Crater, where sharp
 506 boundaries separate morphologically distinct deposits lying side by side on the crater floor.

507 The target material properties affect the formation process in all three crater formation
 508 stages (see section 2.1). In the compression and excavation stages, denser, bulkier material
 509 will naturally better resist the penetrating projectile and the propagating shockwave. In the
 510 modification stage, material strength and porosity become important with bedrock retaining
 511 the crater transient shape better than loosely packed regolith (Dundas et al., 2010; Stopar
 512 et al., 2017).

513 Physical laws linking the target properties, the impactor energy and the crater dimen-
 514 sions were first introduced following experiments conducted on controlled TNT explosions
 515 (Lampson, 1946; Chabai, 1965). These initial studies led to the current extensive, quasi-
 516 experimental crater scaling formalism that links the impact energy and the target properties
 517 to the volume of the transient crater V_t formed on the surface, employing Buckingham’s π
 518 theorem of dimensional analysis (e.g. Holsapple and Schmidt, 1987; Schmidt and Housen,
 519 1987; Holsapple, 1993; Richardson, 2009),

$$V_t = K_1 \left(\frac{m_i}{\rho_t} \right) \left[\left(\frac{ga_i}{v_i^2} \right) \left(\frac{\rho_t}{\rho_i} \right)^{-\frac{1}{3}} + \left(\frac{\bar{Y}}{\rho_t v_i^2} \right)^{\frac{2+\mu}{2}} \right]^{-\frac{3\mu}{2+\mu}} \quad (3)$$

520 where m_i, a_i, v_i and ρ_i are the mass, radius, velocity and density of the impactor, ρ_t is the
 521 target material density, g is the acceleration due to gravity and K_1, \bar{Y} and μ are experi-
 522 mentally derived properties of the target material. \bar{Y} is the target material strength, which
 523 has units of pressure, $1/3 < \mu < 2/3$ is a parameter that affects the physical dimensions of

524 the coupling parameter (see Holsapple and Schmidt, 1987), and determines if the impact is
 525 governed by the impactor momentum ($\mu = 1/3$) or kinetic energy ($\mu = 2/3$) and K_1 is a
 526 proportionality constant. For example, for loose sand $\bar{Y} \sim 0$ Pa, $\mu = 0.41$ and $K_1 = 0.24$
 527 while for hard rock $\bar{Y} \sim 10^7$ Pa, $\mu = 0.55$ and $K_1 = 0.2$. Other typical values for these constants
 528 may be found in Holsapple (1993) and Williams et al. (2014). The crater diameter
 529 may be obtained by taking the cube root of the volume, $V = \pi D^3/24$.

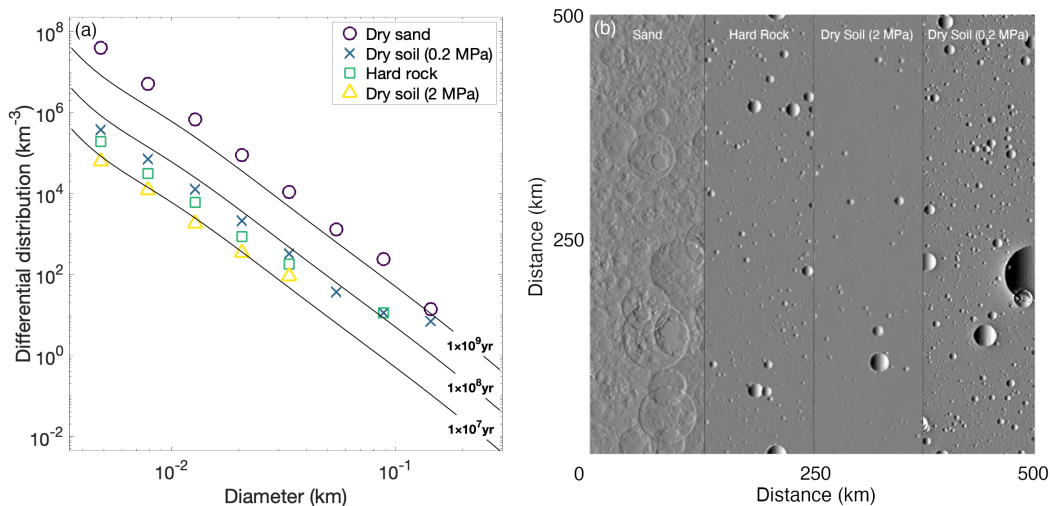


Figure 14: The effect of material properties on the crater size distribution, and the derived age of the surface. We use our Monte Carlo model to simulate an impactor size distribution with $b = 2.5$ for 500 Ma. The results deviate slightly from the isochrons since the power law coefficient we employed assumes the impact rate measured for Earth bolides (Brown et al., 2002), corrected for Mars (Le Feuvre and Wieczorek, 2011). We assume an impactor density of $\rho_i = 1500 \text{ kg m}^{-3}$, an impact velocity of $v_i = 20 \text{ km s}^{-1}$ and $g = 3.7 \text{ m s}^{-2}$. To simulate targets with different material properties, we use parameters from Holsapple (1993). (a) The crater size distribution for four sets of target properties: dry sand ($\mu = 0.41$, $K_1 = 0.24$, $\bar{Y} = 0$ Pa), two types of dry soil ($\mu = 0.41$, $K_1 = 0.24$, $\bar{Y} = 0.2$ and 2 MPa) and hard rock ($\mu = 0.55$, $K_1 = 0.2$, $\bar{Y} = 20$ MPa), with isochrons drawn from the production function due to Ivanov (2001). Even though the impactor size distribution is identical for all surfaces, the derived age is significantly different. (b) Four snapshots showing part of the simulated 500 Ma old surface. Note the different crater size distribution and morphology in each case. The image panels in (b) only show part of the simulated surface as example, and should not be regarded as representative of the complete surface crater size frequency distribution.

530 In order to demonstrate the effect of material strength on the crater size distribution, we
 531 use a Monte Carlo model that is based on the Cratered Terrain Evolution Model (CTEM) by
 532 Richardson (2009). Our model employs π -scaling (Equation 3) and realistic ejecta (Richardson
 533 et al., 2007) to randomly form craters on an initially smooth (without craters) surface
 534 and simulate impact related processes. We choose four example material properties from
 535 Holsapple (1993): dry sand, two types of dry soil, and hard rock. For each set of material
 536 properties, we form crater populations using the same production function: a power law im-

537 pactor size distribution with $b = 2.5$ for 500 Ma (see section 2.1). In all of the simulations,
538 we set the impactor density to $\rho_i = 1500 \text{ kg m}^{-3}$, the impact velocity to $v_i = 20 \text{ kms}^{-1}$ and
539 assume a martian-like $g = 3.7 \text{ m s}^{-2}$.

540 Panel (a) of Figure 14 shows four differential distributions, one for each crater population,
541 along with isochrons from the Ivanov (2001) production function. Even though we employed
542 the same impactor size distribution in forming the craters, their derived age is different
543 by up to two orders of magnitude. In Panel (b) we show four snapshots, one from each
544 simulation, that demonstrate material properties not only change the crater age, but also the
545 morphology of the cratered surface. Our results indicate that the target material properties
546 have a significant effect on the observed crater size distribution - which may help resolve
547 some of the differences between the ages derived from the size distributions we analyzed in
548 section 3.2.

549 4 Discussion and Conclusions

550 Mars' history of surface water and active atmosphere invite challenges that interfere with
551 our ability to reliably date its surface through crater counting. Above we reviewed some of
552 these challenges, adopting as a case study the crater Jezero, the landing site of the Mars
553 2020 mission. Understanding the size distribution of craters within Jezero is important, as
554 the radiometric age of samples obtained from the basin floor could be used in the future to
555 calibrate crater chronology studies on Mars.

556 In order to demonstrate how these challenges affect the measured crater size distributions
557 on the floor of Jezero, we have compiled a catalog of 3274 craters complete to approximately
558 50 – 70 m, depending on the surveyed unit (see Figure 11). Our study focused on comparing
559 the age derived from the crater size distributions to the depositional age of the units derived
560 by interpreting the local geology. Employing crater chronology, we have dated three promi-
561 nent geologic units found within of Jezero Crater: the dark-toned floor unit, the light-toned
562 floor unit and the western delta fan unit. Due to the near absence of craters on the northern
563 fan unit, we were not able to reliably derive its crater age.

564 Of all the geologic units on the floor of Jezero Crater, the dark-toned floor best records
565 and preserves impact craters over time. In order to extend the range of craters previously
566 used to date the unit, we employed bootstrapping to better estimate the rollover diameter
567 of the crater size distribution. The crater age we found for the dark-toned floor unit, $2 \pm$
568 0.07 Ga , is slightly lower than previous estimates (Shahrzad et al., 2019). This discrepancy,
569 along with recent models showing erosion may significantly alter the crater age of limited
570 count regions (Palucis et al., 2020), should be taken into account when calibrating the crater
571 age of the surface of the dark-toned floor with its measured radiometric age.

572 In contrast to the geologic evidence, which may indicate the dark-toned floor unit embays
573 the delta fan units, their crater retention age suggests the former is an order of magnitude
574 older than the latter. Above we have shown that due to extensive erosion, which is in part a
575 function of the material properties, the crater size distribution on the delta fans potentially
576 represents a younger age. This is further bolstered by the presence of Belva Crater that
577 matches the $\sim 3 \text{ Ga}$ isochron and better agrees with the derived depositional age of the unit.
578 This discrepancy demonstrates well that crater chronology is a proxy of the time duration
579 that a surface has been exposed to impactors, rather than the age of the geologic unit, and
580 should always be incorporated with knowledge about the geology of the target material.

581 Unlike the delta fan units, which show extensive erosion, craters on the light-toned floor

582 unit are better preserved and should provide a more accurate estimate of the retention age
583 of the unit. However, once again, the derived model age (1.7 ± 0.3 Ga) disagrees with the
584 superposition relationship of the unit determined from images. Here, the differences could
585 be related to the different material strength of the units. Above we have shown that in
586 some cases the age estimate is heavily influenced by the target material properties that, in
587 the case of craters $\sim 10 - 100$ m, could differ by up to an order of magnitude. This again
588 demonstrates the large errors that may be associated with dating cratered terrains without
589 estimates of the target material properties.

590 Previously, it was postulated (Shahrzad et al., 2019) the large variability in crater density
591 on the floor of Jezero may be related to the presence of a cluster of secondaries. In order
592 to test this hypothesis, we inspected the morphology of craters on the floor of Jezero, but
593 found no clusters or crater chains. Additionally, craters in the area do not appear more
594 elliptical, or located near a large recent primary crater. Instead, we suggest the difference
595 in crater density on the floor of Jezero is probably related to the geology of the delta units.
596 The tone and morphology of the areas with the lowest crater density in Jezero resemble
597 the surface surrounding the delta fan units. This puzzling line of evidence may suggest the
598 west delta fan extended well inside Jezero, protecting the floor underneath it or that the
599 superpositional relationships between the dark-toned floor unit and the delta units are not
600 yet entirely known. It is also likely that wind currents within the basin lofted material that
601 partially covered or buried small craters found east of the delta fragments (see Figure 5).

602 Curiously, the differential distribution of all cratered units within Jezero share a younger
603 power law branch in their size-frequency distribution between $\sim 10-100$ m. This observation
604 is puzzling, and may indicate a widespread geologic resurfacing process has recently (\sim
605 100 Ma) occurred in the crater on a large scale. We note such an event would have to be
606 significant in order to erase these ~ 50 m craters, whose initial depth was likely $\sim 5 - 10$ m,
607 but are unable to present evidence to help us constrain its nature.

608 Acknowledgements

609 The authors wish to thank Nicholas Warner and an anonymous reviewer for helpful feedback
610 and discussion. The contributions of J.-P. Williams were funded by a NASA Solar System
611 Workings grant 80NSSC18K0010.

612 References

- 613 Anders, E. (1965). Fragmentation history of asteroids. *Icarus*, 4(4):399–408.
- 614 Baldwin, R. (1981). On the origin of the planetesimals that produced the multi-ring basins.
615 In *Multi-ring basins: Formation and Evolution*, pages 19–28.
- 616 Baldwin, R. B. (1949). *The face of the moon*. University of Chicago Press.
- 617 Barata, T., Alves, E. I., Saraiva, J., and Pina, P. (2004). Automatic recognition of im-
618 pact craters on the surface of mars. In *International Conference Image Analysis and*
619 *Recognition*, pages 489–496. Springer.
- 620 Baum, M. and Wordsworth, R. (2020). Jezero crater and timing of an early martian ocean.
621 *LPI*, (2326):2490.

- 622 Bierhaus, E., McEwen, A. S., Robbins, S., Singer, K., Dones, L., Kirchoff, M., and Williams,
623 J.-P. (2018). Secondary craters and ejecta across the solar system: Populations and effects
624 on impact-crater-based chronologies. *Meteoritics & Planetary Science*, 53(4):638–671.
- 625 Bierhaus, E. B., Chapman, C. R., and Merline, W. J. (2005). Secondary craters on europa
626 and implications for cratered surfaces. *Nature*, 437(7062):1125–1127.
- 627 Blasius, K. R. (1976). The record of impact cratering on the great volcanic shields of the
628 tharsis region of mars. *Icarus*, 29(3):343–361.
- 629 Brown, H. (1960). The density and mass distribution of meteoritic bodies in the neighbor-
630 hood of the earth’s orbit. *Journal of Geophysical Research*, 65(6):1679–1683.
- 631 Brown, P., Spalding, R., ReVelle, D. O., Tagliaferri, E., and Worden, S. (2002). The flux of
632 small near-earth objects colliding with the earth. *Nature*, 420(6913):294.
- 633 Cabrol, N. A. and Grin, E. A. (1999). Distribution, classification, and ages of martian
634 impact crater lakes. *Icarus*, 142(1):160–172.
- 635 Chabai, A. J. (1965). On scaling dimensions of craters produced by buried explosives.
636 *Journal of Geophysical Research*, 70(20):5075–5098.
- 637 Chappelow, J. E. and Sharpton, V. L. (2006). Atmospheric variations and meteorite pro-
638 duction on mars. *Icarus*, 184(2):424–435.
- 639 Crater Analysis Techniques Working Group (1979). Standard techniques for presentation
640 and analysis of crater size-frequency data. *Icarus*, 37(2):467–474.
- 641 Day, M. and Dorn, T. (2019). Wind in jezero crater, mars. *Geophysical Research Letters*,
642 46(6):3099–3107.
- 643 De Hon, R. (1992). Martian lake basins and lacustrine plains. *Earth, Moon, and Planets*,
644 56(2):95–122.
- 645 Deutsch, A. N., Head, J. W., Chabot, N. L., and Neumann, G. A. (2018). Constraining the
646 thickness of polar ice deposits on mercury using the mercury laser altimeter and small
647 craters in permanently shadowed regions. *Icarus*, 305:139–148.
- 648 Dobra, E. N., Stoker, C., Berman, D., McKay, C., and Davila, A. (2020). Crater morphol-
649 ogy and evolution at the phoenix landing site: Insights into timing of modern geological
650 processes and subsurface ice. *Icarus*, 342:113534.
- 651 Dundas, C. M., Keszthelyi, L. P., Bray, V. J., and McEwen, A. S. (2010). Role of material
652 properties in the cratering record of young platy-ridged lava on mars. *Geophysical Research
653 Letters*, 37(12).
- 654 Edgett, K. S. and Malin, M. C. (2014). Heavily-cratered sedimentary rock occurrences
655 at the surface of mars. In *Abstract 202-1, Geological Society of America Abstracts with
656 Programs*, volume 46.
- 657 Edwards, C., Bandfield, J., Christensen, P., and Rogers, A. (2014). The formation of
658 infilled craters on mars: Evidence for widespread impact induced decompression of the
659 early martian mantle? *Icarus*, 228:149–166.

- 660 Efron, B. and Tibshirani, R. (1985). The bootstrap method for assessing statistical accuracy.
661 *Behaviormetrika*, 12(17):1–35.
- 662 Ehlmann, B. L., Mustard, J. F., Fassett, C. I., Schon, S. C., Head III, J. W., Des Marais,
663 D. J., Grant, J. A., and Murchie, S. L. (2008). Clay minerals in delta deposits and organic
664 preservation potential on mars. *Nature Geoscience*, 1(6):355.
- 665 Fassett, C. I. and Head III, J. W. (2005). Fluvial sedimentary deposits on mars: Ancient
666 deltas in a crater lake in the nili fossae region. *Geophysical Research Letters*, 32(14).
- 667 Fassett, C. I. and Thomson, B. J. (2014). Crater degradation on the lunar maria: Topo-
668 graphic diffusion and the rate of erosion on the moon. *Journal of Geophysical Research:*
669 *Planets*, 119(10):2255–2271.
- 670 Fujiwara, A. and Tsukamoto, A. (1980). Experimental study on the velocity of fragments
671 in collisional breakup. *Icarus*, 44(1):142–153.
- 672 Gault, D., Hörz, F., Brownlee, D., and Hartung, J. (1974). Mixing of the lunar regolith. In
673 *Lunar and Planetary Science Conference Proceedings*, volume 5, pages 2365–2386.
- 674 Golder, K., Miklusick, N., Spaulding, R., Atkins, J., Boring, B., Hicks, T., Shaver, E.,
675 and Kah, L. (2020). Behavioral characteristics of dark-toned crater floor materials, jezero
676 crater: Implications for mode of emplacement. *LPI*, (2326):1302.
- 677 Goudge, T. A., Head, J. W., Mustard, J. F., and Fassett, C. I. (2012). An analysis of open-
678 basin lake deposits on mars: Evidence for the nature of associated lacustrine deposits and
679 post-lacustrine modification processes. *Icarus*, 219(1):211–229.
- 680 Goudge, T. A., Milliken, R. E., Head, J. W., Mustard, J. F., and Fassett, C. I. (2017). Sedi-
681 mentological evidence for a deltaic origin of the western fan deposit in jezero crater, mars
682 and implications for future exploration. *Earth and Planetary Science Letters*, 458:357–365.
- 683 Goudge, T. A., Mohrig, D., Cardenas, B. T., Hughes, C. M., and Fassett, C. I. (2018).
684 Stratigraphy and paleohydrology of delta channel deposits, jezero crater, mars. *Icarus*,
685 301:58–75.
- 686 Goudge, T. A., Mustard, J. F., Head, J. W., Fassett, C. I., and Wiseman, S. M. (2015).
687 Assessing the mineralogy of the watershed and fan deposits of the jezero crater paleolake
688 system, mars. *Journal of Geophysical Research: Planets*, 120(4):775–808.
- 689 Grant, J. A., Golombek, M. P., Wilson, S. A., Farley, K. A., Williford, K. H., and Chen,
690 A. (2018). The science process for selecting the landing site for the 2020 mars rover.
691 *Planetary and Space Science*, 164:106–126.
- 692 Greeley, R. and Gault, D. E. (1970). Precision size-frequency distributions of craters for 12
693 selected areas of the lunar surface. *The Moon*, 2(1):10–77.
- 694 Greeley, R. and Gault, D. E. (1971). Endogenetic craters interpreted from crater counts on
695 the inner wall of copernicus. *Science*, 171(3970):477–479.
- 696 Grotzinger, J. P. and Milliken, R. E. (2012). The sedimentary rock record of mars: Distri-
697 bution, origins, and global stratigraphy. *Sedimentary Geology of Mars*, 102:1–48.

- 698 Hartmann, W. (1964). On the distribution of lunar crater diameters. *Communications of*
699 *the Lunar and Planetary Laboratory*, 2:197–204.
- 700 Hartmann, W. and Daubar, I. (2017). Martian cratering 11. utilizing decameter scale crater
701 populations to study martian history. *Meteoritics & Planetary Science*, 52(3):493–510.
- 702 Hartmann, W. K. (1966). Martian cratering. *Icarus*, 5(1-6):565–576.
- 703 Hartmann, W. K. (1981). Chronology of planetary volcanism by comparative studies of
704 planetary cratering. *Basaltic Volcanism on the Terrestrial Planets.*, pages 1049–1127.
- 705 Hartmann, W. K. (1999). Martian cratering vi: Crater count isochrons and evidence for
706 recent volcanism from mars global surveyor. *Meteoritics & Planetary Science*, 34(2):167–
707 177.
- 708 Hartmann, W. K. (2005). Martian cratering 8: Isochron refinement and the chronology of
709 mars. *Icarus*, 174(2):294–320.
- 710 Hartmann, W. K. and Hartmann, A. C. (1968). Asteroid collisions and evolution of aster-
711 oidal mass distribution and meteoritic flux. *Icarus*, 8(1-3):361–381.
- 712 Hartmann, W. K. and Neukum, G. (2001). Cratering chronology and the evolution of mars.
713 In *Chronology and evolution of Mars*, pages 165–194. Springer.
- 714 Hawkins, G. S. (1960). Asteroidal fragments. *The Astronomical Journal*, 65:318.
- 715 Holsapple, K. (1993). The scaling of impact processes in planetary sciences. *Annual review*
716 *of earth and planetary sciences*, 21(1):333–373.
- 717 Holsapple, K. and Schmidt, R. (1987). Point source solutions and coupling parameters in
718 cratering mechanics. *Journal of Geophysical Research: Solid Earth*, 92(B7):6350–6376.
- 719 Irwin III, R. P. and Zimbelman, J. R. (2012). Morphometry of great basin pluvial shore
720 landforms: Implications for paleolake basins on mars. *Journal of Geophysical Research:*
721 *Planets*, 117(E7).
- 722 Ivanov, B., Deniem, D., and Neukum, G. (1997). Implementation of dynamic strength
723 models into 2d hydrocodes: Applications for atmospheric breakup and impact cratering.
724 *International Journal of Impact Engineering*, 20(1-5):411–430.
- 725 Ivanov, B. A. (2001). Mars/moon cratering rate ratio estimates. *Space Science Reviews*,
726 96(1-4):87–104.
- 727 Kah, L., Scheller, E., Eide, S., Meyen, F., Jacob, S., Spaulding, R., Miklusicak, N., Golder,
728 K., and Stack-Morgan, K. (2020). Depositional relationships between crater floor mate-
729 rials in jezero crater, mars. *LPI*, (2326):1301.
- 730 Kreiter, T. (1960). Dating lunar surface features by using crater frequencies. *Publications*
731 *of the Astronomical Society of the Pacific*, 72(428):393–398.
- 732 Lampson, C. J. (1946). Explosions in earth. *Effects of Impact and Explosions*, 1(2):110.
- 733 Lapôtre, M. G. and Ielpi, A. (2020). The pace of fluvial meanders on mars and implications
734 for the western delta deposits of jezero crater. *AGU Advances*, 1(2):e2019AV000141.

- 735 Le Feuvre, M. and Wieczorek, M. A. (2011). Nonuniform cratering of the moon and a
736 revised crater chronology of the inner solar system. *Icarus*, 214(1):1–20.
- 737 Lorenz, R. D. and Lunine, J. I. (1996). Erosion on titan: Past and present. *Icarus*, 122(1):79–
738 91.
- 739 Mainzer, A., Grav, T., Masiero, J., Bauer, J., Cutri, R., McMillan, R., Nugent, C., Tholen,
740 D., Walker, R., and Wright, E. (2012). Physical parameters of asteroids estimated from the
741 wise 3-band data and neowise post-cryogenic survey. *The Astrophysical Journal Letters*,
742 760(1):L12.
- 743 Malin, M. C., Bell, J. F., Cantor, B. A., Caplinger, M. A., Calvin, W. M., Clancy, R. T.,
744 Edgett, K. S., Edwards, L., Haberle, R. M., James, P. B., et al. (2007). Context camera
745 investigation on board the mars reconnaissance orbiter. *Journal of Geophysical Research:*
746 *Planets*, 112(E5).
- 747 Malin, M. C., Edgett, K. S., Cantor, B. A., Caplinger, M. A., Danielson, G. E., Jensen,
748 E. H., Ravine, M. A., Sandoval, J. L., and Supulver, K. D. (2010). An overview of the
749 1985–2006 mars orbiter camera science investigation. *Mars*, 5:1–60.
- 750 Marchi, S., Mottola, S., Cremonese, G., Massironi, M., and Martellato, E. (2009). A new
751 chronology for the moon and mercury. *The Astronomical Journal*, 137(6):4936.
- 752 Massey, F. J. (1951). The kolmogorov-smirnov test for goodness of fit. *Journal of the*
753 *American statistical Association*, 46(253):68–78.
- 754 McEwen, A. S., Eliason, E. M., Bergstrom, J. W., Bridges, N. T., Hansen, C. J., Delamere,
755 W. A., Grant, J. A., Gulick, V. C., Herkenhoff, K. E., Keszthelyi, L., et al. (2007). Mars
756 reconnaissance orbiter’s high resolution imaging science experiment (hirise). *Journal of*
757 *Geophysical Research: Planets*, 112(E5).
- 758 McEwen, A. S., Preblich, B. S., Turtle, E. P., Artemieva, N. A., Golombek, M. P., Hurst,
759 M., Kirk, R. L., Burr, D. M., and Christensen, P. R. (2005). The rayed crater zumil and
760 interpretations of small impact craters on mars. *Icarus*, 176(2):351–381.
- 761 Melosh, H. J. (1989). *Impact cratering: A geologic process*. Oxford University Press.
- 762 Michael, G. (2013). Planetary surface dating from crater size–frequency distribution
763 measurements: Multiple resurfacing episodes and differential isochron fitting. *Icarus*,
764 226(1):885–890.
- 765 Michael, G., Kneissl, T., and Neesemann, A. (2016). Planetary surface dating from crater
766 size-frequency distribution measurements: Poisson timing analysis. *Icarus*, 277:279 – 285.
- 767 Michael, G. and Neukum, G. (2010). Planetary surface dating from crater size–frequency dis-
768 tribution measurements: Partial resurfacing events and statistical age uncertainty. *Earth*
769 *and Planetary Science Letters*, 294(3-4):223–229.
- 770 Milton, D. J. (1973). Water and processes of degradation in the martian landscape. *Journal*
771 *of Geophysical Research*, 78(20):4037–4047.
- 772 Neukum, G. (1984). Meteorite bombardment and dating of planetary surfaces.

- 773 Neukum, G. and Ivanov, B. (1994). Crater size distributions and impact probabilities on
774 earth from lunar, terrestrial-planet, and asteroid cratering data. *Hazards due to Comets
775 and Asteroids*, 1:359–416.
- 776 Neukum, G., Ivanov, B. A., and Hartmann, W. K. (2001). Cratering records in the inner
777 solar system in relation to the lunar reference system. In *Chronology and evolution of
778 Mars*, pages 55–86. Springer.
- 779 Neukum, G., König, B., Fechtig, H., and Storzer, D. (1975). Cratering in the earth-moon
780 system-consequences for age determination by crater counting. In *Lunar and Planetary
781 Science Conference Proceedings*, volume 6, pages 2597–2620.
- 782 Palucis, M. C., Jasper, J., Garczynski, B., and Dietrich, W. E. (2020). Quantitative assess-
783 ment of uncertainties in modeled crater retention ages on mars. *Icarus*, 341:113623.
- 784 Pasckert, J. H., Hiesinger, H., and van der Bogert, C. H. (2015). Small-scale lunar farside
785 volcanism. *Icarus*, 257:336–354.
- 786 Popova, O., Nemtchinov, I., and Hartmann, W. K. (2003). Bolides in the present and past
787 martian atmosphere and effects on cratering processes. *Meteoritics & Planetary Science*,
788 38(6):905–925.
- 789 Preblich, B. S., McEwen, A. S., and Studer, D. M. (2007). Mapping rays and secondary
790 craters from the martian crater zunil. *Journal of Geophysical Research: Planets*, 112(E5).
- 791 Quantin, C., Popova, O., Hartmann, W. K., and Werner, S. C. (2016). Young martian crater
792 gratteri and its secondary craters. *Journal of Geophysical Research: Planets*, 121(7):1118–
793 1140.
- 794 Rabinowitz, D. (1993). The size distribution of the earth-approaching asteroids. *The As-
795 trophysical Journal*, 407:412–427.
- 796 Richardson, J. E. (2009). Cratering saturation and equilibrium: A new model looks at an
797 old problem. *Icarus*, 204(2):697–715.
- 798 Richardson, J. E., Melosh, H. J., Lisse, C. M., and Carcich, B. (2007). A ballistics analysis of
799 the deep impact ejecta plume: Determining comet tempel 1’s gravity, mass, and density.
800 *Icarus*, 191(2):176–209.
- 801 Richardson Jr, J. E., Melosh, H. J., Greenberg, R. J., and O’Brien, D. P. (2005). The global
802 effects of impact-induced seismic activity on fractured asteroid surface morphology. *Icarus*,
803 179(2):325–349.
- 804 Robbins, S. J. (2019). A new global database of lunar impact craters \geq 1–2 km: 1. crater
805 locations and sizes, comparisons with published databases, and global analysis. *Journal
806 of Geophysical Research: Planets*, 124(4):871–892.
- 807 Robbins, S. J. and Hynes, B. M. (2011). Secondary crater fields from 24 large primary
808 craters on mars: Insights into nearby secondary crater production. *Journal of Geophysical
809 Research: Planets*, 116(E10).
- 810 Robbins, S. J. and Hynes, B. M. (2012a). A new global database of mars impact craters \geq 1
811 km: 1. database creation, properties, and parameters. *Journal of Geophysical Research:
812 Planets*, 117.

- 813 Robbins, S. J. and Hynek, B. M. (2012b). A new global database of mars impact craters \geq 1
814 km: 2. global crater properties and regional variations of the simple-to-complex transition
815 diameter. *Journal of Geophysical Research: Planets*, 117(E6).
- 816 Robbins, S. J. and Hynek, B. M. (2014). The secondary crater population of mars. *Earth
817 and Planetary Science Letters*, 400:66–76.
- 818 Rubanenko, L., Venkatraman, J., and Paige, D. A. (2019). Thick ice deposits in shallow
819 simple craters on the moon and mercury. *Nature Geoscience*, 12(8):597–601.
- 820 Salese, F., Kleinhans, M. G., Mangold, N., Ansan, V., McMahon, W., de Haas, T., and
821 Dromart, G. (2020). Estimated minimum life span of the jezero fluvial delta (mars).
822 *Astrobiology*.
- 823 Schmidt, R. M. and Housen, K. R. (1987). Some recent advances in the scaling of impact
824 and explosion cratering. *International Journal of Impact Engineering*, 5(1-4):543–560.
- 825 Schon, S. C., Head, J. W., and Fassett, C. I. (2012). An overfilled lacustrine system and
826 progradational delta in jezero crater, mars: Implications for noachian climate. *Planetary
827 and Space Science*, 67(1):28–45.
- 828 Schultz, P. H. and Singer, J. (1980). A comparison of secondary craters on the moon,
829 mercury, and mars. In *Lunar and Planetary Science Conference Proceedings*, volume 11,
830 pages 2243–2259.
- 831 Schuyler, A., Warner, N., Derick, B., Rogers, A., and Golombek, M. (2020). Crater mor-
832 phometry on the dark-toned mafic floor unit at jezero crater, mars: Comparisons to a
833 known basaltic lava plain at the insight landing site. *LPI*, (2326):1608.
- 834 Shahrzad, S., Kinch, K. M., Goudge, T. A., Fassett, C. I., Needham, D. H., Quantin-Nataf,
835 C., and Knudsen, C. P. (2019). Crater statistics on the dark-toned, mafic floor unit in
836 jezero crater, mars. *Geophysical Research Letters*, 46(5):2408–2416.
- 837 Shoemaker, E. M. (1965). Preliminary analysis of the fine structure of the lunar surface in
838 mare cognitum. In *The nature of the lunar surface*, page 23.
- 839 Silburt, A., Ali-Dib, M., Zhu, C., Jackson, A., Valencia, D., Kissin, Y., Tamayo, D., and
840 Menou, K. (2019). Lunar crater identification via deep learning. *Icarus*, 317:27–38.
- 841 Smith, D. E., Zuber, M. T., Frey, H. V., Garvin, J. B., Head, J. W., Muhleman, D. O.,
842 Pettengill, G. H., Phillips, R. J., Solomon, S. C., Zwally, H. J., et al. (2001). Mars orbiter
843 laser altimeter: Experiment summary after the first year of global mapping of mars.
844 *Journal of Geophysical Research: Planets*, 106(E10):23689–23722.
- 845 Smith, M. R., Gillespie, A. R., and Montgomery, D. R. (2008). Effect of obliteration on
846 crater-count chronologies for martian surfaces. *Geophysical research letters*, 35(10).
- 847 Soderblom, L., Condit, C., West, R. A., Herman, B., and Kreidler, T. (1974). Martian
848 planetwide crater distributions: Implications for geologic history and surface processes.
849 *Icarus*, 22(3):239–263.
- 850 Spencer, L. J. (1937). Meteorites and the craters on the moon.

- 851 Stepinski, T. F., Mendenhall, M. P., and Bue, B. D. (2009). Machine cataloging of impact
852 craters on mars. *icarus*, 203(1):77–87.
- 853 Stöffler, D. and Ryder, G. (2001). Stratigraphy and isotope ages of lunar geologic units:
854 Chronological standard for the inner solar system. In *Chronology and evolution of Mars*,
855 pages 9–54. Springer.
- 856 Stopar, J. D., Robinson, M. S., Barnouin, O. S., McEwen, A. S., Speyerer, E. J., Henriksen,
857 M. R., and Sutton, S. S. (2017). Relative depths of simple craters and the nature of the
858 lunar regolith. *Icarus*, 298:34–48.
- 859 Strom, R. G., Banks, M. E., Chapman, C. R., Fassett, C. I., Forde, J. A., Head III, J. W.,
860 Merline, W. J., Prockter, L. M., and Solomon, S. C. (2011). Mercury crater statistics
861 from messenger flybys: Implications for stratigraphy and resurfacing history. *Planetary
862 and Space Science*, 59(15):1960–1967.
- 863 Stuart, J. S. and Binzel, R. P. (2004). Bias-corrected population, size distribution, and
864 impact hazard for the near-earth objects. *Icarus*, 170(2):295–311.
- 865 Sweeney, J., Warner, N., Ganti, V., Golombek, M., Lamb, M., Ferguson, R., and Kirk, R.
866 (2018). Degradation of 100-m-scale rocky ejecta craters at the insight landing site on mars
867 and implications for surface processes and erosion rates in the hesperian and amazonian.
868 *Journal of Geophysical Research: Planets*, 123(10):2732–2759.
- 869 Warner, N., Grant, J., Wilson, S., Golombek, M., DeMott, A., Charalambous, C., Hauber,
870 E., Ansan, V., Weitz, C., Pike, T., et al. (2020). An impact crater origin for the in-
871 sight landing site at homestead hollow, mars: Implications for near surface stratigra-
872 phy, surface processes, and erosion rates. *Journal of Geophysical Research: Planets*,
873 125(4):e2019JE006333.
- 874 Warner, N. H., Gupta, S., Calef, F., Grindrod, P., Boll, N., and Goddard, K. (2015).
875 Minimum effective area for high resolution crater counting of martian terrains. *Icarus*,
876 245:198–240.
- 877 Wilhelms, D. (1976). Secondary impact craters of lunar basins. In *Lunar and Planetary
878 Science Conference Proceedings*, volume 7, pages 2883–2901.
- 879 Williams, J.-P., Pathare, A. V., and Aharonson, O. (2014). The production of small primary
880 craters on mars and the moon. *Icarus*, 235:23–36.
- 881 Williams, J.-P., van der Bogert, C. H., Pathare, A. V., Michael, G. G., Kirchoff, M. R.,
882 and Hiesinger, H. (2018). Dating very young planetary surfaces from crater statistics: A
883 review of issues and challenges. *Meteoritics & Planetary Science*, 53(4):554–582.
- 884 Williford, K. H., Farley, K. A., Stack, K. M., Allwood, A. C., Beaty, D., Beegle, L. W.,
885 Bhartia, R., Brown, A. J., de la Torre Juarez, M., Hamran, S.-E., et al. (2018). The nasa
886 mars 2020 rover mission and the search for extraterrestrial life. In *From Habitability to
887 Life on Mars*, pages 275–308. Elsevier.
- 888 Young, J. (1940). A statistical investigation of diameter and distribution of lunar craters.
889 *J. Brit. Astron. Assoc.*, 50(9):309–326.